

---

# Causal Neural Probabilistic Circuits

---

Weixin Chen<sup>1</sup>

Han Zhao<sup>1</sup>

<sup>1</sup>University of Illinois Urbana-Champaign, IL, USA

## Abstract

Concept Bottleneck Models (CBMs) enhance the interpretability of end-to-end neural networks by introducing a layer of concepts and predicting the class label from the concept predictions. A key property of CBMs is that they support interventions, *i.e.*, domain experts can correct mispredicted concept values at test time to improve the final accuracy. However, typical CBMs apply interventions by overwriting only the corrected concept while leaving other concept predictions unchanged, which ignores causal dependencies among concepts. To address this, we propose the Causal Neural Probabilistic Circuit (CNPC), which combines a neural attribute predictor with a causal probabilistic circuit compiled from a causal graph. This circuit supports exact, tractable causal inference that inherently respects causal dependencies. Under interventions, CNPC models the class distribution based on a Product of Experts (PoE) that fuses the attribute predictor’s predictive distribution with the interventional marginals computed by the circuit. We theoretically characterize the compositional interventional error of CNPC *w.r.t.* its modules and identify conditions under which CNPC closely matches the ground-truth interventional class distribution. Experiments on five benchmark datasets in both in-distribution and out-of-distribution settings show that, compared with five baseline models, CNPC achieves higher task accuracy across different numbers of intervened attributes.

## 1 INTRODUCTION

Despite achieving high performance across a range of benchmarks [Deng et al., 2009, Wang et al., 2019], deep learning models are often black-box and lack interpretability [Rudin,

2019], which makes it difficult to understand why a specific decision is made, let alone to interact with the decision process. Concept Bottleneck Models (CBMs) [Koh et al., 2020, Stammer et al., 2021] offer a promising direction by introducing a concept layer that decomposes the decision process into two stages: a neural concept predictor first infers human-understandable concepts from the input, and a label predictor, often a linear layer, then maps the predicted concepts to the final class label. This architecture provides concept-level explanations and, more importantly, supports interventions, *i.e.*, a human can correct any mispredicted concept values. Such interventions are particularly valuable in safety-critical applications such as medical diagnosis [Esteva et al., 2017, De Fauw et al., 2018], where a domain expert can inspect and correct concept values to improve the accuracy and reliability of the final prediction.

In practice, however, typical CBMs [Koh et al., 2020, Zarlenga et al., 2022, Oikarinen et al., 2023] implement interventions by overwriting only the corrected concept while leaving all other concept predictions unchanged; see Figure 1 (top panel). It ignores the causal dependencies among concepts, where intervening on one concept could lead to updates on other concepts that depend on it [Pearl, 2009, Peters et al., 2017]. For example, knowing that a patient smokes should increase the likelihood of lung cancer. Therefore, to improve intervention efficiency and make better use of costly expert interventions, CBMs should propagate interventions through the causal structure over concepts and the class label, yielding the interventional class distribution for updated prediction.

In this paper, however, we show that exactly modeling this interventional class distribution is challenging in CBMs: the interventional attribute<sup>1</sup> distribution cannot, in general, be obtained using the standard CBM modules. To address this

---

<sup>1</sup>In the CBM literature, a *concept* is defined as a binary variable indicating the presence or absence of a human-interpretable property (*e.g.*, *is\_red\_color*, *is\_yellow\_color*), whereas we use a more general term *attribute*, defined as a categorical variable that takes values from a finite set of such properties (*e.g.*, *color*).

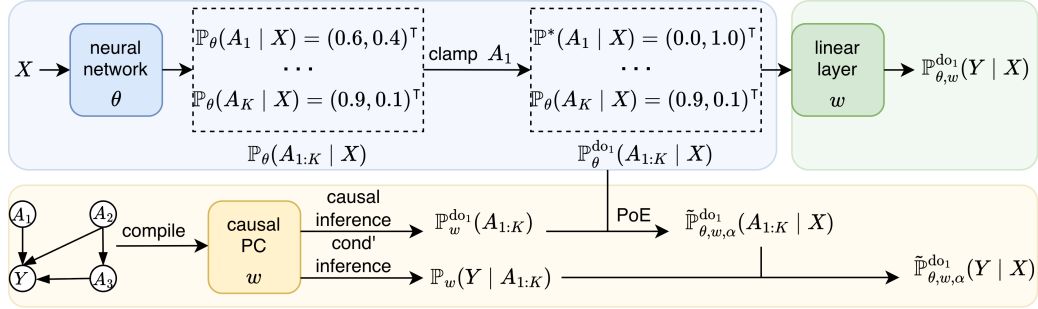


Figure 1: A typical CBM (top left module + top right module) performs the intervention on  $A_1$  by replacing the neural network’s predictions for  $A_1$  with the ground-truth distribution, while leaving the predictions for other attributes unchanged. In contrast, CNPC (top left module + bottom module) combines a neural network with a causal PC compiled from a causal graph, and approximates the interventional class distribution based on a PoE with a balancing weight  $\alpha$  that fuses complementary information from the two modules.

challenge, inspired by the recent Neural Probabilistic Circuit (NPC) [Chen et al., 2025a,b], we propose the Causal Neural Probabilistic Circuit (CNPC). An NPC consists of a neural attribute predictor and a probabilistic circuit (PC) [Poon and Domingos, 2011, Choi et al., 2020, Vergari et al., 2020] that performs exact, tractable probabilistic inference over attributes and the class label. It predicts the class distribution by combining the predicted attribute distribution and the conditional distribution of the class label given attributes computed by the PC. We extend NPC to CNPC by additionally compiling a causal graph over attributes and the class label into the PC, yielding a causal PC [Darwiche, 2022] that supports exact, tractable probabilistic and causal inference. When there is no intervention, CNPC uses the same prediction form as NPC. Under interventions on one or more attributes, we approximate the interventional attribute distribution using a Product of Experts (PoE) [Hinton, 2002] that combines the neural predictor’s attribute distribution with the interventional marginal attribute distribution computed exactly by the causal PC. CNPC then predicts the class distribution by combining this PoE-based approximation with the conditional distribution of the class label given attributes computed by the causal PC.

Our theoretical results show that both NPC and CNPC exhibit compositional errors *w.r.t.* the neural predictor and the PC under interventions; moreover, under certain conditions, CNPC matches the ground-truth interventional class distribution more closely than NPC. To empirically evaluate CNPC, we consider four settings: one benign (in-distribution) setting and three out-of-distribution (OOD) settings where the test-time input distribution deviates from the training distribution. The OOD settings include unseen data transformations [Hendrycks and Dietterich, 2019b], adversarial perturbations [Goodfellow et al., 2015], and spurious-correlation shifts [Arjovsky et al., 2019]. In these OOD settings, the neural predictor may perform unreliably, thus necessitating interventions. Empirical results for CNPC and five baseline models across five benchmark datasets show three main findings. First, task accuracy increases for all models as the number of intervened attributes grows,

demonstrating the effectiveness of interventions. Second, in the benign setting, all models perform similarly, with CNPC achieving a small advantage on most datasets. Third, in the OOD settings, CNPC substantially outperforms all baselines across different numbers of intervened attributes, indicating its high efficiency in utilizing interventions.

Our contributions are summarized as follows. **(1)** We propose CNPC, which combines a neural attribute predictor with a causal PC and approximates the interventional class distribution using a PoE. **(2)** We provide theoretical results characterizing the compositional interventional errors of NPC and CNPC, and show that CNPC can model the ground-truth interventional class distribution more accurately than NPC under certain conditions. **(3)** We empirically show that CNPC achieves higher intervention efficiency compared with various baseline models, especially in OOD settings.

## 2 RELATED WORK

**Modeling Concept Dependencies in CBMs.** Traditional CBMs [Koh et al., 2020] predict each concept independently from the input, which neglects dependencies among concepts. Modeling such dependencies can be useful, especially under intervention, as one can update the values of remaining concepts given an intervened concept. A representative approach is SCBM [Vandenhirtz et al., 2024], which models values of all concepts with a multivariate normal distribution and trains two neural networks to predict the mean vector and covariance matrix from the input, respectively. The interventional concept distribution is derived by conditioning the multivariate normal on the intervened concepts. Similarly, Havasi et al. [2022] leverage an auto-regressive model to capture concept dependencies. Moreover, de Felice et al. [2025], Dominici et al. [2025] model causal dependencies among concepts by incorporating a ground-truth or learned causal structure into the concept predictor, where neural networks are trained to approximate the underlying structural equations. Accordingly, each concept prediction depends on the predictions of its causal ancestors, and interventions are propagated through the causal structure.

**Intervention Strategies.** Due to the high cost of human interventions, the number of concepts that can be intervened on is often limited. This naturally raises the question of which concepts to select under a fixed intervention budget. Ideally, an intervention strategy should choose the concepts that yield the largest improvement in downstream task performance. Shin et al. [2023], Sheth et al. [2022] study a range of selection criteria (*e.g.*, prediction uncertainty) as well as different selection granularities (*e.g.*, intervening on individual concepts versus concept groups). They find that no single criterion is consistently best across settings, and that intervening on concept groups can be cost-effective when concepts within a group are mutually exclusive. Henceforth, interventions are performed by default on concept groups, *i.e.*, attributes. Beyond these hand-crafted selection criteria, Chauhan et al. [2023], Steinmann et al. [2024] learn policies that adaptively choose the next concept to intervene on. With the incorporation of an explicit causal graph, de Felice et al. [2025] perform interventions in a top-down manner along the causal hierarchy, as intervening on higher-level attributes can potentially influence more downstream attributes. In this work, we follow de Felice et al. [2025] and select attributes by their depth in the causal graph. However, it remains unclear whether this strategy is the most intervention-efficient for CNPC. We leave it as a future direction and discuss it in Appendix A.

### 3 PRELIMINARIES

#### 3.1 NOTATION AND ASSUMPTIONS

CBMs predict the class label solely through the predicted concept values, which relies on the following assumption:

**Assumption 1** (Sufficient Attributes [Chen et al., 2025a]). The class label  $Y$  and the input  $X$  are conditionally independent given the attributes  $A_{1:K}$ , *i.e.*,  $Y \perp X \mid A_{1:K}$ .

In the case of insufficient attributes, one may leverage Large Language Models (LLMs) or Vision-Language Models (VLMs) for automated concept discovery and labeling [Oikarinen et al., 2023, Yüsekçönlü et al., 2023, Srivastava et al., 2024], which is an active research problem in the CBM literature. While this is complementary to our method, here we assume that sufficient attributes are annotated, as our main focus is the incorporation of causal dependencies.

We also assume access to the structure of a causal graph  $\mathcal{C}^2$  over the semantically meaningful, observable variables, *i.e.*, attributes  $A_{1:K}$  and the class label  $Y$ . Each node in the graph represents a variable, and each directed edge  $V_1 \rightarrow V_2$  indicates that  $V_1$  is a causal parent (direct cause) of  $V_2$ . We assume there are no unobserved confounders among the

<sup>2</sup>We assume access only to the graph structure, while the specific causal mechanisms can remain unknown.

variables in  $\mathcal{C}$ . For a random variable  $V \in \mathcal{C}$ , we use  $\text{Pa}_{\mathcal{C}}(V)$  to denote the parent nodes of  $V$  in  $\mathcal{C}$  and  $\text{ND}_{\mathcal{C}}(V)$  to denote the non-descendants of  $V$  in  $\mathcal{C}$ , respectively. Throughout the paper, we make the following structural assumption of  $\mathcal{C}$ :

**Assumption 2** (Structural assumption of the causal graph).  $\text{Pa}_{\mathcal{C}}(Y) \subseteq \{A_{1:K}\} \subseteq \text{ND}_{\mathcal{C}}(Y)$ .

The availability of the graph structure is a common assumption in causal inference [Pearl, 1995, 2009, Tian and Pearl, 2002] and is typically obtained from domain knowledge. When it is unknown, one may apply existing causal discovery algorithms [Spirtes and Glymour, 1991, Heckerman et al., 1995, Chickering, 2002] to learn a plausible graph.

#### 3.2 NEURAL PROBABILISTIC CIRCUITS

A Neural Probabilistic Circuit (NPC) consists of two modules. The first is an attribute predictor, which is a neural network with  $K$  classification heads and parameterized by  $\theta$ . It takes an input  $X$  and predicts  $K$  attribute distributions  $\{\mathbb{P}_{\theta}(A_k \mid X)\}_{k=1}^K$ . The second is a probabilistic circuit (PC) [Choi et al., 2020], specifically a sum-product network [Poon and Domingos, 2011], parameterized by  $w$ . It represents the joint distribution  $\mathbb{P}_w(Y, A_{1:K})$  while supporting the tractable computation of the conditional distribution  $\mathbb{P}_w(Y \mid A_{1:K})$ . Combining these two modules, NPC predicts the class distribution as:

$$\mathbb{P}_{\theta,w}(Y \mid X) = \sum_{a_{1:K}} \mathbb{P}_w(Y \mid A_{1:K} = a_{1:K}) \cdot \prod_{k=1}^K \mathbb{P}_{\theta}(A_k = a_k \mid X). \quad (1)$$

Although not explicitly described in the original paper, the interventional distribution modeled by NPC can be inferred from the standard intervention procedure used in CBMs. Consider an intervention on attribute  $A_j$ . NPC would replace the  $j$ -th predicted attribute distribution with the ground truth  $\mathbb{P}_*(A_j \mid X)$  while leaving the remaining distributions unchanged. Consequently, NPC models the interventional class distribution under intervention on  $A_j$  as:

$$\begin{aligned} \mathbb{P}_{\theta,w}^{\text{do}_j}(Y \mid X) &= \sum_{a_{1:K}} \mathbb{P}_w(Y \mid A_{1:K} = a_{1:K}) \cdot \mathbb{P}_{\theta}^{\text{do}_j}(A_{1:K} = a_{1:K} \mid X), \\ \mathbb{P}_{\theta}^{\text{do}_j}(A_{1:K} = a_{1:K} \mid X) &= \mathbb{P}_*(A_j = a_j \mid X) \cdot \prod_{k \neq j} \mathbb{P}_{\theta}(A_k = a_k \mid X). \end{aligned} \quad (2)$$

This formulation naturally extends to interventions on multiple attributes.

#### 3.3 CAUSAL PROBABILISTIC CIRCUITS

Traditional approaches to causal inference for interventional queries reduce to exact inference on the mutilated graph (the causal graph with incoming edges into intervened variables deleted) induced by the intervention [Pearl, 2010], and hence have a complexity that is exponential in

treewidth [Dechter, 1999, Koller and Friedman, 2009, Darwiche, 2009]. In contrast, Chavira and Darwiche [2007], Darwiche [2020, 2022] show that a symbolic causal graph can be compiled into a PC, specifically an arithmetic circuit [Darwiche, 2021], that supports exact causal inference in time linear in circuit size.

In particular, they use the Variable Elimination (VE) algorithm [Koller and Friedman, 2009] to schedule factor operations within the network polynomial [Darwiche, 2003], and construct an arithmetic circuit accordingly. As an example, consider three variables with the graph structure  $V_2 \leftarrow V_1 \rightarrow V_3$ . Each variable corresponds to a factor that represents its conditional probability distribution (CPD):  $\phi_{V_1}(V_1)$ ,  $\phi_{V_2}(V_1, V_2)$ , and  $\phi_{V_3}(V_1, V_3)$ , whose symbolic entries are  $\phi_{v_1}$ ,  $\phi_{v_2|v_1}$ , and  $\phi_{v_3|v_1}$ , respectively. Each variable is also associated with an evidence factor,  $\lambda_{V_i}(V_i)$ , with entries given by indicator functions  $\lambda_{v_i} = \mathbb{I}(V_i = v_i)$ . With these notations, the network polynomial is expressed as:

$$f(\phi, \lambda) = \sum_{v_1, v_2, v_3} \phi_{v_1} \phi_{v_2|v_1} \phi_{v_3|v_1} \lambda_{v_1} \lambda_{v_2} \lambda_{v_3}.$$

Given an elimination order, *e.g.*,  $[V_2, V_3, V_1]$ , VE schedules the factor operations (multiplication and sum-out), yielding an equivalent expression that is more efficient to evaluate [Dechter, 1999, Zhang and Poole, 1996]:

$$f(\phi, \lambda) = \sum_{v_1} \phi_{v_1} \lambda_{v_1} \cdot \left( \sum_{v_3} \phi_{v_3|v_1} \lambda_{v_3} \right) \cdot \left( \sum_{v_2} \phi_{v_2|v_1} \lambda_{v_2} \right).$$

See the full derivation in Appendix B.1.

An arithmetic circuit is then constructed by establishing a sum node for the sum-out operator while establishing a product node for the multiplication operator. For simplicity, suppose all variables are binary<sup>3</sup>, and we use  $v_i$  and  $\bar{v}_i$  to denote  $V_i = 1$  and  $V_i = 0$ . The resulting circuit is illustrated in Figure 2. We refer to this circuit that compiles the causal graph as the *causal PC*. For the values of those symbolic entries, one can use gradient descent or EM to seek maximum-likelihood estimates [Darwiche, 2022].

As the causal PC encodes the network polynomial, it supports tractable probabilistic inference [Darwiche, 2003]. Computing the probability of any joint or marginal event, *e.g.*,  $\Pr(v_1, \bar{v}_2)$ , only requires setting the indicators whose subscript is compatible with the event to 1, *i.e.*,  $\lambda_{v_1} = 1$ ,  $\lambda_{\bar{v}_2} = 1$ ,  $\lambda_{v_3} = 1$ ,  $\lambda_{\bar{v}_3} = 1$ , and enabling one forward pass in PC. Conditional inference, hence, requires two PC forward passes. In addition, with the compilation of the causal graph, the causal PC also supports tractable causal inference. Computing the interventional probability<sup>4</sup>, *e.g.*,  $\Pr^{\text{do}(\bar{v}_2)}(v_1)$ , can be done in two steps: (i) Replace the CPD entries of the intervened variable with 1, *i.e.*,  $\phi_{v_2|v_1} = 1$ ,

<sup>3</sup>The extension to the categorical ones is standard.

<sup>4</sup>The causal PC also supports tractable inference for counterfactual queries. As it is out of the scope of this paper, we do not discuss the details here.

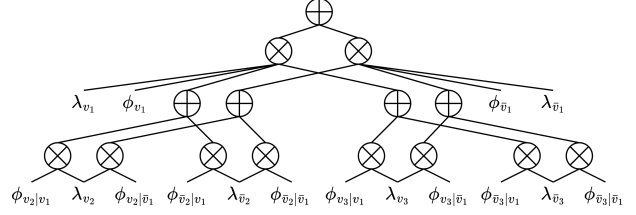


Figure 2: A PC that compiles the causal graph  $V_2 \leftarrow V_1 \rightarrow V_3$ .

$\phi_{v_2|\bar{v}_1} = 1$ ,  $\phi_{\bar{v}_2|v_1} = 1$ ,  $\phi_{\bar{v}_2|\bar{v}_1} = 1$ ; (ii) Set the indicators compatible with  $(v_1, \bar{v}_2)$  to 1. Following these two steps, the causal PC outputs  $\Pr^{\text{do}(\bar{v}_2)}(v_1) = \phi_{v_1} = \Pr(v_1)$ , which is the expected result as  $V_2$  has no causal effect on  $V_1$ .

## 4 METHOD

### 4.1 WHY IS MODELING THE INTERVENTIONAL CLASS DISTRIBUTION HARD

Given an input  $X$ , the interventional class distribution under  $\text{do}_j$ , which fixes the value of  $A_j$  according to  $\mathbb{P}_*(A_j | X)$ <sup>5</sup>, can be written as:

$$\begin{aligned} \mathbb{P}^{\text{do}_j}(Y | X) &= \sum_{a_{1:K}} \mathbb{P}^{\text{do}_j}(Y | A_{1:K} = a_{1:K}) \cdot \mathbb{P}^{\text{do}_j}(A_{1:K} = a_{1:K} | X), \\ &= \sum_{a_{1:K}} \mathbb{P}(Y | \text{Pa}_C(Y) = a_{1:K} | \text{Pa}_C(Y)) \cdot \mathbb{P}^{\text{do}_j}(A_{1:K} = a_{1:K} | X), \\ &= \sum_{a_{1:K}} \mathbb{P}(Y | A_{1:K} = a_{1:K}) \cdot \mathbb{P}^{\text{do}_j}(A_{1:K} = a_{1:K} | X). \end{aligned} \quad (3)$$

The first equality follows from the law of total probability and Assumption 1. The second step applies Assumption 2 alongside the invariance of the causal mechanism for  $Y$  [Peters et al., 2017]. Finally, the last equality holds by reapplying Assumption 2 under the local Markov property.

In Eq. (3), the first term can be evaluated exactly and tractably by the (causal) PC. The second term, however, is not directly available from any module. Using the Bayes' rule, we can further rewrite it as:

$$\mathbb{P}^{\text{do}_j}(A_{1:K} = a_{1:K} | X) \propto \mathbb{P}^{\text{do}_j}(A_{1:K} = a_{1:K}) \cdot \mathbb{P}^{\text{do}_j}(X | A_{1:K} = a_{1:K}).$$

In a simplistic setting where  $\text{Pa}_C(X) = \{A_{1:K}\}$ ,  $\mathbb{P}^{\text{do}_j}(X | A_{1:K}) = \mathbb{P}(X | A_{1:K})$  by invariance of causal mechanisms. Consequently,  $\mathbb{P}^{\text{do}_j}(A_{1:K} = a_{1:K} | X)$  simplifies to:

$$\mathbb{P}^{\text{do}_j}(A_{1:K} = a_{1:K} | X) \propto \frac{\mathbb{P}^{\text{do}_j}(A_{1:K} = a_{1:K})}{\mathbb{P}(A_{1:K} = a_{1:K})} \cdot \mathbb{P}(A_{1:K} = a_{1:K} | X).$$

Here, the ratio term can be computed via causal and probabilistic inference in the causal PC, while  $\mathbb{P}(A_{1:K} = a_{1:K} | X)$  can be provided by the neural attribute predictor. Hence,  $\mathbb{P}^{\text{do}_j}(Y | X)$  can be computed using these two components.

Nevertheless, we typically do not know the causal relationships between the high-dimensional input  $X$  and other

<sup>5</sup> $\mathbb{P}_*(A_j | X)$  is  $\mathbb{I}(A_j = a_j^*(X))$  for some  $a_j^*(X) \in \mathcal{A}_j$ .

variables, and  $\mathbb{P}^{\text{do}_j}(X \mid A_{1:K})$  does not coincide with  $\mathbb{P}(X \mid A_{1:K})$  in general. This mismatch can arise, for example, if  $X$  has additional (possibly unobserved) causal parents beyond  $A_{1:K}$ , or if some attributes in  $A_{1:K}$  are descendants of  $X$ . Therefore, modeling  $\mathbb{P}^{\text{do}_j}(X \mid A_{1:K})$  would require learning an interventional generative model for  $X$ , which is challenging, as many powerful generative models (e.g., diffusion models [Ho et al., 2020] and GANs [Goodfellow et al., 2020]) do not allow access to the generative probabilities but only sampling, and we do not have access to the interventional samples of  $X$ .

## 4.2 CAUSAL NEURAL PROBABILISTIC CIRCUITS

To address the aforementioned challenge, we propose the Causal Neural Probabilistic Circuit (CNPC), which consists of an attribute predictor and a causal PC; see the bottom panel in Figure 1. Similar to NPC, the attribute predictor is a multi-head neural network that predicts the  $K$  attributes from the input, and is trained with standard supervised learning. The causal PC is obtained by compiling the causal graph over the attributes and the class label, and its parameters are given by the maximum-likelihood estimates.

Under interventions, to approximate the intractable term  $\mathbb{P}^{\text{do}_j}(A_{1:K} \mid X)$  in Eq. (3), *i.e.*, the ground-truth interventional attribute distribution, CNPC uses a Product of Experts (PoE) that combines complementary information from the two modules. Consider the intervention  $\text{do}_j$ . The two experts used by CNPC are: **(i)** the attribute distribution predicted by the neural predictor with  $A_j$  clamped to its ground-truth distribution, *i.e.*,  $\mathbb{P}_\theta^{\text{do}_j}(A_{1:K} \mid X) = \mathbb{P}_*(A_j \mid X) \cdot \prod_{k \neq j} \mathbb{P}_\theta(A_k \mid X)$ , and **(ii)** the interventional marginal over attributes computed exactly by the causal PC, *i.e.*,  $\mathbb{P}_w^{\text{do}_j}(A_{1:K})$ . The PoE approximation is defined as:

$$\tilde{\mathbb{P}}_{\theta,w,\alpha}^{\text{do}_j}(A_{1:K} \mid X) = \frac{\left(\mathbb{P}_\theta^{\text{do}_j}(A_{1:K} \mid X)\right)^{1-\alpha} \left(\mathbb{P}_w^{\text{do}_j}(A_{1:K})\right)^\alpha}{Z_\alpha(X)}, \quad (4)$$

where  $Z_\alpha(X)$  is the normalizing constant and  $\alpha \in [0, 1]$  is a balancing weight that controls the relative influence of the two experts.<sup>6</sup>

The use of PoE preserves the evidence from the input through the neural predictor, while also accounting for how intervening on one attribute affects the others, since the causal PC performs exact interventional inference, essentially the inference on the mutilated graph.

With the PoE approximation, CNPC predicts the interven-

tional class distribution as follows:

$$\tilde{\mathbb{P}}_{\theta,w,\alpha}^{\text{do}_j}(Y \mid X) = \sum_{a_{1:K}} \mathbb{P}_w(Y \mid A_{1:K} = a_{1:K}) \cdot \tilde{\mathbb{P}}_{\theta,w,\alpha}^{\text{do}_j}(A_{1:K} = a_{1:K} \mid X). \quad (5)$$

When there is no intervention, CNPC predicts the class distribution in the same way as NPC, *i.e.*, via Eq. (1). Furthermore, when  $\alpha = 0$ , CNPC reduces to NPC.

## 5 THEORETICAL ANALYSIS

In this section, we present theoretical results to understand the behavior of NPC and CNPC with and without intervention. Proofs are deferred to Appendix D.

First, analogous to Chen et al. [2025a, Theorem 2], Theorem 3 shows that both the prediction errors of CNPC and NPC admit a compositional bound in terms of the errors of the attribute predictor and the PC. Hence, improving either module can improve the overall predictive distribution.

**Theorem 3.** *The expected prediction error of NPC (CNPC), measured by KL divergence, is upper-bounded by the sum of the expected prediction error of the attribute predictor and that of the PC (causal PC). Specifically,*

$$\begin{aligned} & \mathbb{E}_{X \sim \mathbb{P}_*} [\text{KL}(\mathbb{P}_*(Y \mid X) \parallel \mathbb{P}_{\theta,w}(Y \mid X))] \\ & \leq \mathbb{E}_{X \sim \mathbb{P}_*} [\text{KL}(\mathbb{P}_*(A_{1:K} \mid X) \parallel \mathbb{P}_\theta(A_{1:K} \mid X))] \\ & \quad + \mathbb{E}_{A_{1:K} \sim \mathbb{P}_*} [\text{KL}(\mathbb{P}_*(Y \mid A_{1:K}) \parallel \mathbb{P}_w(Y \mid A_{1:K}))]. \end{aligned}$$

*Equality holds if for each  $(x, y)$ , there exists a constant  $c(x, y)$  s.t.  $\frac{\mathbb{P}_*(a_{1:K} \mid x) \mathbb{P}_*(y \mid a_{1:K})}{\mathbb{P}_\theta(a_{1:K} \mid x) \mathbb{P}_w(y \mid a_{1:K})} = c(x, y)$  for all  $a_{1:K}$ .*

Corollary 4 and 5 show that a similar compositional error decomposition still holds under interventions.

**Corollary 4.** *The expected interventional error of NPC is upper-bounded by the sum of the expected interventional error of the attribute predictor and the expected prediction error of the PC. Specifically,*

$$\begin{aligned} & \mathbb{E}_{X \sim \mathbb{P}_*^{\text{do}_j}} \left[ \text{KL} \left( \mathbb{P}_*^{\text{do}_j}(Y \mid X) \parallel \mathbb{P}_{\theta,w}^{\text{do}_j}(Y \mid X) \right) \right] \\ & \leq \mathbb{E}_{X \sim \mathbb{P}_*^{\text{do}_j}} \left[ \text{KL} \left( \mathbb{P}_*^{\text{do}_j}(A_{1:K} \mid X) \parallel \mathbb{P}_\theta^{\text{do}_j}(A_{1:K} \mid X) \right) \right] \\ & \quad + \mathbb{E}_{A_{1:K} \sim \mathbb{P}_*^{\text{do}_j}} [\text{KL}(\mathbb{P}_*(Y \mid A_{1:K}) \parallel \mathbb{P}_w(Y \mid A_{1:K}))]. \end{aligned}$$

*Equality holds if for each  $(x, y)$ , there exists a constant  $c(x, y)$  s.t.  $\frac{\mathbb{P}_*^{\text{do}_j}(a_{1:K} \mid x) \mathbb{P}_*(y \mid a_{1:K})}{\mathbb{P}_\theta^{\text{do}_j}(a_{1:K} \mid x) \mathbb{P}_w(y \mid a_{1:K})} = c(x, y)$  for all  $a_{1:K}$ .*

**Corollary 5.** *The expected interventional error of CNPC is upper-bounded by a weighted sum of (i) the expected interventional error of the attribute predictor, (ii) the expected interventional error of the causal PC over attributes, and (iii) the expected prediction error of the causal PC. Specifically,*

$$\begin{aligned} & \mathbb{E}_{X \sim \mathbb{P}_*^{\text{do}_j}} \left[ \text{KL} \left( \mathbb{P}_*^{\text{do}_j}(Y \mid X) \parallel \tilde{\mathbb{P}}_{\theta,w,\alpha}^{\text{do}_j}(Y \mid X) \right) \right] \\ & \leq (1 - \alpha) \mathbb{E}_{X \sim \mathbb{P}_*^{\text{do}_j}} \left[ \text{KL} \left( \mathbb{P}_*^{\text{do}_j}(A_{1:K} \mid X) \parallel \mathbb{P}_\theta^{\text{do}_j}(A_{1:K} \mid X) \right) \right] \\ & \quad + \alpha \mathbb{E}_{X \sim \mathbb{P}_*^{\text{do}_j}} \left[ \text{KL} \left( \mathbb{P}_*^{\text{do}_j}(A_{1:K} \mid X) \parallel \mathbb{P}_w^{\text{do}_j}(A_{1:K}) \right) \right] \\ & \quad + \mathbb{E}_{A_{1:K} \sim \mathbb{P}_*^{\text{do}_j}} [\text{KL}(\mathbb{P}_*(Y \mid A_{1:K}) \parallel \mathbb{P}_w(Y \mid A_{1:K}))]. \end{aligned}$$

<sup>6</sup>The extension to interventions on multiple attributes is straightforward, as we only need to clamp the intervened attributes to their ground-truth distributions and compute the corresponding interventional marginal using the causal PC.

Equality holds if for each  $(x, y)$ ,  $\mathbb{P}_\theta^{do_j}(a_{1:K} \mid x) = \mathbb{P}_w^{do_j}(a_{1:K})$  for all  $a_{1:K}$ , and there exists a constant  $c(x, y)$

s.t.  $\frac{\mathbb{P}_*^{do_j}(a_{1:K} \mid x) \mathbb{P}_*(y \mid a_{1:K})}{\mathbb{P}_\theta^{do_j}(a_{1:K} \mid x) \mathbb{P}_w(y \mid a_{1:K})} = c(x, y)$  for all  $a_{1:K}$ .

**Remark.** Let  $\mathbb{B}_{NPC}$  and  $\mathbb{B}_{CNPC}$  denote the interventional error bounds of NPC and CNPC, respectively. It follows directly that if

$$\text{KL}(\mathbb{P}_*^{do_j}(A_{1:K} \mid X) \parallel \mathbb{P}_w^{do_j}(A_{1:K})) \leq \text{KL}(\mathbb{P}_*^{do_j}(A_{1:K} \mid X) \parallel \mathbb{P}_\theta^{do_j}(A_{1:K} \mid X)),$$

then  $\mathbb{B}_{CNPC} \leq \mathbb{B}_{NPC}$ . This indicates that, when the attribute predictor is inaccurate or when the interventional marginal is close to the ground-truth interventional attribute distribution, CNPC may perform better than NPC.

## 6 EXPERIMENTS

### 6.1 EXPERIMENTAL SETTINGS

**Datasets.** We evaluate our approach on five datasets spanning diverse domains. **(1) Asia:** Asia [Lauritzen and Spiegelhalter, 1988] is originally a Bayesian network for medical diagnosis from bnlearn [Scutari, 2010]. We sample 10,000 data points, using the value of the “dysp” node as the class label and values of the remaining nodes as attribute labels. Following de Felice et al. [2025], we train an autoencoder to map the attribute labels into an embedding, which serves as the input to CBMs. We split the dataset into training, validation, and test sets using an 80:10:10 ratio. **(2) Sachs:** Similar to Asia, Sachs [Sachs et al., 2005] is a Bayesian network for biological signaling from bnlearn. We follow the same procedure to obtain the corresponding dataset. Because neither Asia nor Sachs contains image data, we use them exclusively in the benign setting. **(3) MNISTAdd:** Each instance in MNISTAdd comprises two digit images from MNIST [LeCun et al., 2002]. The digit values serve as attribute labels, and their sum forms the class label. We generate 50,000 instances by sampling labels from a predefined causal Bayesian network and concatenating the corresponding randomly sampled MNIST images. We then split the data using an 80:10:10 ratio. The standard test set is used for the benign setting. It is then applied with 180-degree rotations and PGD attacks [Madry et al., 2018], respectively, to construct two OOD variants. **(4) cMNISTAdd:** Unlike MNISTAdd, cMNISTAdd introduces spurious correlations using colored digits. In the training and validation sets, the digits 0–9 are spuriously correlated with a specific list of colors; in the test set, this digit-to-color mapping is reversed. We use this dataset exclusively in the OOD setting to evaluate robustness against these spurious correlations. **(5) CelebA:** CelebA [Liu et al., 2015] comprises 202,599 celebrity face images annotated with 40 highly imbalanced binary attributes. We restrict our focus to the five most balanced attributes, defining the class label as a

unique combination of attribute labels (yielding 32 distinct classes). Additionally, we manually annotate the underlying causal graph. The data is split using the 80:10:10 ratio. As with MNISTAdd, we apply 180-degree rotations and PGD attacks to the test set to generate OOD variants.

**Baselines.** We select five representative CBMs as our baselines: **(1) Vanilla CBM** [Koh et al., 2020] consists of a standard neural concept predictor followed by a linear label predictor. **(2) CEM** [Zarlenga et al., 2022] utilizes high-dimensional concept embeddings rather than scalar concept predictions for its label predictor to enhance downstream task performance. **(3) SCBM** [Vandenhirtz et al., 2024] models the joint distribution of all concepts using a multivariate normal distribution and treats interventions as conditional distributions. **(4) C<sup>2</sup>BM** [de Felice et al., 2025] integrates a causal graph into the concept predictor, allowing interventions to propagate through the graph structure. **(5) NPC** [Chen et al., 2025a] employs a PC as the label predictor to exactly encode the probabilistic dependencies among attributes and the class label.

**Implementation.** For a fair evaluation, CNPC and all baseline models employ Multi-Layer Perceptrons (MLPs) as their neural predictors. Following de Felice et al. [2025], we determine the attribute intervention order based on node depth in the causal graph, *i.e.*, the longest directed path from the root nodes. All baseline models adhere to this order. Further implementation details are deferred to Appendix C.1.

### 6.2 MAIN RESULTS

We evaluate models under a benign setting (Section 6.2.1) and three distinct OOD scenarios: unseen data transformations (Section 6.2.2), adversarial perturbations (Section 6.2.3), and spurious-correlation shifts (Section 6.2.4).

#### 6.2.1 Benign Performance

In the benign setting, where the test and training distributions are identical, the neural predictor is typically reliable. Thus, we uniformly set  $\alpha = 0.1$  for CNPC across all datasets, placing greater emphasis on the evidence from the input through the neural predictor. A comprehensive ablation study analyzing the effect of varying  $\alpha$  is presented in Section 6.3. Figure 9 in Appendix C.2.1 and Figure 3 illustrate the attribute and task accuracy of CNPC and baseline models on the Asia, Sachs, MNISTAdd, and CelebA datasets under varying numbers of attribute interventions.

Across all four datasets, all models exhibit an upward trend in task accuracy as the number of intervened attributes increases. Such consistency demonstrates the fundamental effectiveness of interventions in concept bottleneck models, also revealing the interpretability of these models as their

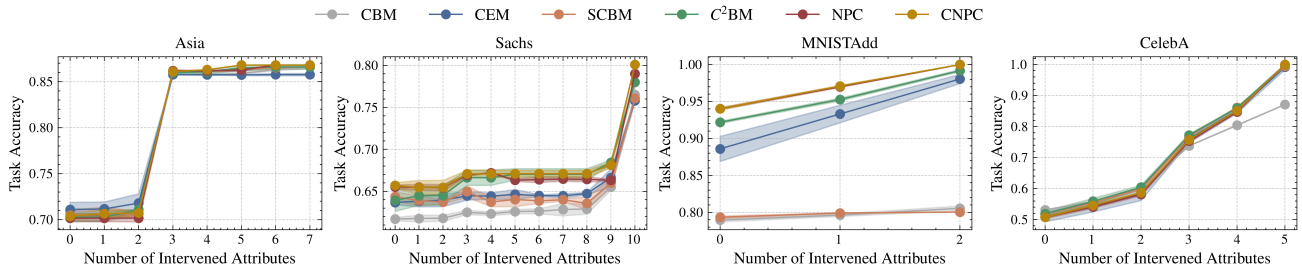


Figure 3: Task accuracy of CNPC and baseline models in the benign setting on the Asia, Sachs, MNISTAdd, and CelebA datasets under varying numbers of attribute interventions. All results are averaged across three random seeds.

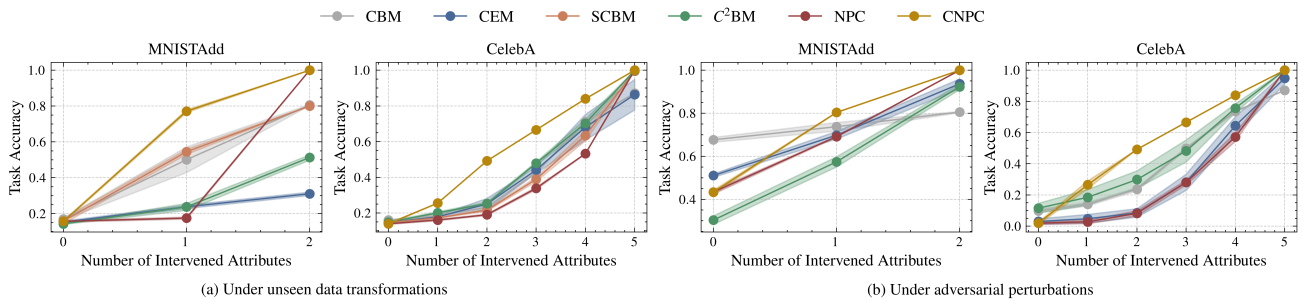


Figure 4: Task accuracy of CNPC and baseline models in OOD settings on the MNISTAdd and CelebA datasets under varying numbers of attribute interventions. All results are averaged across three random seeds.

response to interventions aligns with human expectations.

Notably, on the MNISTAdd dataset, CNPC achieves the highest task accuracy across all numbers of intervened attributes. On the remaining datasets, all models behave similarly, with CNPC and  $C^2$ BM marginally leading in most cases. This result suggests that by leveraging the underlying causal relationships among attributes and the class label, the intervention efficiency can be improved.

## 6.2.2 Performance against Unseen Data Transformations

Neural networks are notoriously vulnerable to OOD shifts [Hendrycks and Dietterich, 2019a]. We consider such a scenario by applying a data transformation unseen during training on test instances, specifically a 180-degree rotation. We uniformly set  $\alpha = 0.9$  for CNPC across all datasets, placing greater emphasis on the evidence from causal dependencies through the causal PC. Figure 10 (a) in Appendix C.2.2 and Figure 4 (a) illustrate the attribute and task accuracy of CNPC and the baseline models on MNISTAdd and CelebA under varying numbers of attribute interventions.

As anticipated, the unseen transformation severely degrades the attribute accuracy of all models. Specifically, without interventions, the attribute accuracy drops from over 92% to below 20% on MNISTAdd, and from over 85% to about 50% on CelebA. In this scenario, interventions therefore become crucial for recovering downstream task performance.

On both datasets, CNPC consistently outperforms all baseline models by a substantial margin across different numbers

of intervened attributes. For instance, CNPC surpasses the second-best model by 22% on MNISTAdd with one intervened attribute, and by 24% on CelebA with two intervened attributes. These results highlight CNPC’s exceptional intervention efficiency under unseen transformations, also suggesting that the interventional distribution computed by the causal PC is important for correcting the final prediction.

## 6.2.3 Performance against Adversarial Perturbations

Here, we investigate a different type of OOD shifts: adversarial perturbations. Specifically, we employ the standard PGD attack to corrupt the neural predictor’s predictions for all attributes. We do not include experiments for SCBM here because it relies on non-differentiable discrete sampling for concept predictions and cannot be directly applied with the gradient-based PGD attack. We still set  $\alpha = 0.9$  for CNPC. Figure 10 (b) in Appendix C.2.2 and Figure 4 (b) illustrate the attribute and task accuracy of CNPC and the baseline models on MNISTAdd and CelebA under varying numbers of attribute interventions.

As observed with unseen data transformations, adversarial perturbations significantly degrade the attribute accuracy of all models. Recall that without any interventions, CNPC reduces to NPC. We note that their task accuracy before interventions is relatively low compared to other baselines. However, despite this inferior initial state, CNPC effectively capitalizes on interventions and ultimately achieves the highest task accuracy across all numbers of attribute interventions. These results further corroborate CNPC’s high efficiency in utilizing interventions.

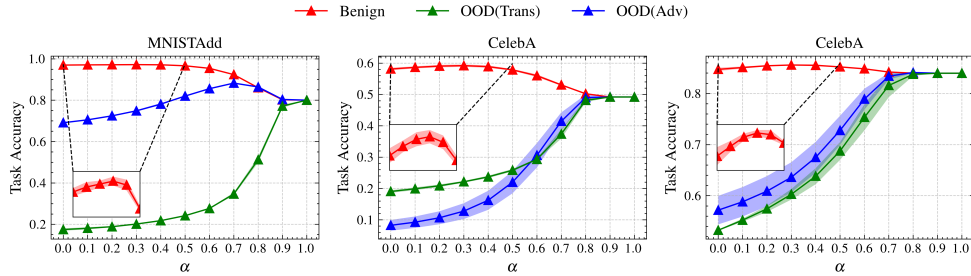


Figure 5: Task accuracy of CNPC in both benign and OOD settings with  $\alpha$  varying from 0.0 to 1.0 in increments of 0.1. **Left:** Performance on MNISTAdd with one intervened attribute. **Middle:** Performance on CelebA with two intervened attributes. **Right:** Performance on CelebA with four intervened attributes. All results are averaged across three random seeds.

### 6.2.4 Performance against Spurious-Correlation Shifts

It is common that deep neural networks exploit spurious correlations, capturing unintended relationships between background features and the target label. We use the cMNISTAdd dataset to investigate model performance against this OOD shift, where digit values are spuriously correlated with colors. We still set  $\alpha = 0.9$  for CNPC. Figure 6 illustrates the attribute and task accuracy of CNPC and baseline models under varying numbers of attribute interventions.

As observed with the previous OOD shifts, the presence of spurious correlations severely reduces the attribute accuracy of all models, while CNPC still leads in task accuracy across varying numbers of attribute interventions.

Furthermore, we find that under all evaluated OOD shifts, the task accuracy of CNPC consistently surpasses that of NPC across various datasets and varying numbers of attribute interventions (except when fully intervened, where both reach 100% accuracy). This sustained improvement underscores the benefits of compiling the underlying causal graph into PC and validates our theoretical analysis as well.

## 6.3 ABLATION STUDIES

**Effect of  $\alpha$ .** By construction,  $\alpha$  in our PoE formulation balances the evidence from the input via the neural predictor against the interventional marginals computed by the causal PC. A larger  $\alpha$  places greater emphasis on the latter.

In the main experiments, we uniformly set  $\alpha = 0.1$  for benign settings and  $\alpha = 0.9$  for OOD settings. However, does a smaller (larger)  $\alpha$  always yield better performance in the benign (OOD) setting? To better understand the effect of  $\alpha$  on CNPC’s performance, we conduct a systematic study. Figure 5 illustrates CNPC’s task accuracy with varying  $\alpha$  across three scenarios: MNISTAdd with one intervened attribute, and CelebA with two and four intervened attributes.

In the benign setting, the task accuracy initially increases and then decreases as  $\alpha$  grows, with the peak accuracy achieved at  $\alpha = 0.3$  in all three scenarios. It is worth noting that in these scenarios, the neural predictor achieves near-

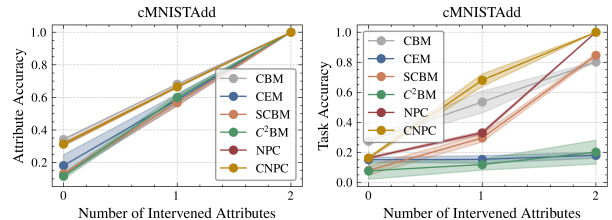


Figure 6: Attribute and task accuracy of CNPC and baseline models on cMNISTAdd under varying numbers of attribute interventions. All results are averaged across three random seeds.

perfect attribute accuracy. Together, these findings suggest that even when the neural predictor is highly reliable, it is not optimal to rely on it exclusively (*i.e.*, by setting  $\alpha$  to its smallest value). Instead, judiciously incorporating causal evidence from the causal PC can improve performance.

Under unseen data transformations, task accuracy monotonically increases. Under adversarial attacks, task accuracy exhibits a similar inverted-U pattern as in the benign setting, albeit peaking much later. Notably, the peak accuracy is achieved at  $\alpha = 0.7$  on MNISTAdd and  $\alpha = 0.8$  on CelebA with four intervened attributes. These results indicate that even when the neural predictor is compromised, it is unwise to discard its evidence entirely. Retaining a modest degree of evidence from the input helps enhance performance.

These observations naturally raise a follow-up question: *Is there a mechanism to adaptively select the optimal  $\alpha$  for a given sample?* We discuss this possibility in Appendix A.

## 7 CONCLUSIONS

To exploit the causal relationships among attributes, we propose CNPC, a model that combines a neural predictor with a PC compiled from a causal graph and estimates the interventional distribution via a PoE. Both theoretical and empirical evidence show that CNPC effectively improves the intervention efficiency over NPC, especially under OOD settings. More broadly, CNPC highlights a practical way to incorporate causal information into predictive models and to approximate causal inference within these models. Limitations and potential solutions are discussed in Appendix A.

## References

- Martin Arjovsky, Léon Bottou, Ishaan Gulrajani, and David Lopez-Paz. Invariant risk minimization. *arXiv preprint arXiv:1907.02893*, 2019.
- Kushal Chauhan, Rishabh Tiwari, Jan Freyberg, Pradeep Shenoy, and Krishnamurthy Dvijotham. Interactive concept bottleneck models. In *Thirty-Seventh AAAI Conference on Artificial Intelligence (AAAI)*, pages 5948–5955. AAAI Press, 2023.
- Mark Chavira and Adnan Darwiche. Compiling bayesian networks using variable elimination. In *Proceedings of the 20th International Joint Conference on Artificial Intelligence IJCAI*, pages 2443–2449, 2007.
- Weixin Chen, Simon Yu, Huajie Shao, Lui Sha, and Han Zhao. Neural probabilistic circuits: Enabling compositional and interpretable predictions through logical reasoning. *arXiv preprint arXiv:2501.07021*, 2025a.
- Weixin Chen, Simon Yu, Huajie Shao, Lui Sha, and Han Zhao. Neural probabilistic circuits: An overview. In *Eighth Workshop on Tractable Probabilistic Modeling*, 2025b.
- David Maxwell Chickering. Optimal structure identification with greedy search. *Journal of machine learning research*, 3(Nov):507–554, 2002.
- Y Choi, Antonio Vergari, and Guy Van den Broeck. Probabilistic circuits: A unifying framework for tractable probabilistic models. *UCLA*. URL: <http://starai.cs.ucla.edu/papers/ProbCirc20.pdf>, page 6, 2020.
- Adnan Darwiche. A differential approach to inference in bayesian networks. *J. ACM*, 50(3):280–305, 2003.
- Adnan Darwiche. *Modeling and reasoning with Bayesian networks*. Cambridge university press, 2009.
- Adnan Darwiche. An advance on variable elimination with applications to tensor-based computation. In *24th European Conference on Artificial Intelligence ECAI*, volume 325 of *Frontiers in Artificial Intelligence and Applications*, pages 2559–2568. IOS Press, 2020.
- Adnan Darwiche. Tractable boolean and arithmetic circuits. In *Neuro-Symbolic Artificial Intelligence: The State of the Art*, pages 146–172. IOS Press, 2021.
- Adnan Darwiche. Causal inference using tractable circuits. *arXiv preprint arXiv:2202.02891*, 2022.
- Jeffrey De Fauw, Joseph R Ledsam, Bernardino Romera-Paredes, Stanislav Nikolov, Nenad Tomasev, Sam Blackwell, Harry Askham, Xavier Glorot, Brendan O’Donoghue, Daniel Visentin, et al. Clinically applicable deep learning for diagnosis and referral in retinal disease. *Nature medicine*, 24(9):1342–1350, 2018.
- Giovanni de Felice, Arianna Casanova Flores, Francesco De Santis, Silvia Santini, Johannes Schneider, Pietro Barbiero, and Alberto Termine. Causally reliable concept bottleneck models. In *Advances in Neural Information Processing Systems 39: Annual Conference on Neural Information Processing Systems (NeurIPS)*, 2025.
- Rina Dechter. Bucket elimination: A unifying framework for reasoning. *Artificial Intelligence*, 113(1-2):41–85, 1999.
- Jia Deng, Wei Dong, Richard Socher, Li-Jia Li, Kai Li, and Li Fei-Fei. Imagenet: A large-scale hierarchical image database. In *IEEE Computer Society Conference on Computer Vision and Pattern Recognition (CVPR)*, pages 248–255. IEEE Computer Society, 2009.
- Gabriele Dominici, Pietro Barbiero, Mateo Espinosa Zarlenga, Alberto Termine, Martin Gjoreski, Giuseppe Marra, and Marc Langheinrich. Causal concept graph models: Beyond causal opacity in deep learning. In *The Thirteenth International Conference on Learning Representations, ICLR 2025, Singapore, April 24-28, 2025*. OpenReview.net, 2025.
- Andre Esteva, Brett Kuperl, Roberto A. Novoa, Justin Ko, Susan M. Swetter, Helen M. Blau, and Sebastian Thrun. Dermatologist-level classification of skin cancer with deep neural networks. *Nat.*, 542(7639):115–118, 2017.
- Robert Gens and Pedro M. Domingos. Learning the structure of sum-product networks. In *ICML*, pages 873–880, 2013.
- Ian Goodfellow, Jean Pouget-Abadie, Mehdi Mirza, Bing Xu, David Warde-Farley, Sherjil Ozair, Aaron Courville, and Yoshua Bengio. Generative adversarial networks. *Communications of the ACM*, 63(11):139–144, 2020.
- Ian J. Goodfellow, Jonathon Shlens, and Christian Szegedy. Explaining and harnessing adversarial examples. In *3rd International Conference on Learning Representations, ICLR*, 2015.
- Marton Havasi, Sonali Parbhoo, and Finale Doshi-Velez. Addressing leakage in concept bottleneck models. In *Advances in Neural Information Processing Systems 35: Annual Conference on Neural Information Processing Systems (NeurIPS)*, 2022.
- David Heckerman, Dan Geiger, and David M Chickering. Learning bayesian networks: The combination of knowledge and statistical data. *Machine learning*, 20(3):197–243, 1995.
- Dan Hendrycks and Thomas G. Dietterich. Benchmarking neural network robustness to common corruptions and perturbations. In *7th International Conference on Learning Representations (ICLR)*. OpenReview.net, 2019a.

- Dan Hendrycks and Thomas G. Dietterich. Benchmarking neural network robustness to common corruptions and perturbations. In *7th International Conference on Learning Representations, ICLR 2019, New Orleans, LA, USA, May 6-9, 2019*. OpenReview.net, 2019b.
- Dan Hendrycks and Kevin Gimpel. A baseline for detecting misclassified and out-of-distribution examples in neural networks. In *5th International Conference on Learning Representations (ICLR)*. OpenReview.net, 2017.
- Geoffrey E Hinton. Training products of experts by minimizing contrastive divergence. *Neural computation*, 14(8):1771–1800, 2002.
- Jonathan Ho, Ajay Jain, and Pieter Abbeel. Denoising diffusion probabilistic models. In *Advances in Neural Information Processing Systems 33: Annual Conference on Neural Information Processing Systems (NeurIPS)*, 2020.
- Pang Wei Koh, Thao Nguyen, Yew Siang Tang, Stephen Mussmann, Emma Pierson, Been Kim, and Percy Liang. Concept bottleneck models. In *Proceedings of the 37th International Conference on Machine Learning, ICML*, volume 119 of *Proceedings of Machine Learning Research*, pages 5338–5348. PMLR, 2020.
- Daphne Koller and Nir Friedman. *Probabilistic graphical models: principles and techniques*. MIT press, 2009.
- Steffen L Lauritzen and David J Spiegelhalter. Local computations with probabilities on graphical structures and their application to expert systems. *Journal of the Royal Statistical Society: Series B (Methodological)*, 50(2):157–194, 1988.
- Yann LeCun, Léon Bottou, Yoshua Bengio, and Patrick Haffner. Gradient-based learning applied to document recognition. *Proceedings of the IEEE*, 86(11):2278–2324, 2002.
- Shiyu Liang, Yixuan Li, and R. Srikant. Enhancing the reliability of out-of-distribution image detection in neural networks. In *6th International Conference on Learning Representations (ICLR)*. OpenReview.net, 2018.
- Ziwei Liu, Ping Luo, Xiaogang Wang, and Xiaoou Tang. Deep learning face attributes in the wild. In *Proceedings of the IEEE international conference on computer vision (CVPR)*, pages 3730–3738, 2015.
- Aleksander Madry, Aleksandar Makelov, Ludwig Schmidt, Dimitris Tsipras, and Adrian Vladu. Towards deep learning models resistant to adversarial attacks. In *ICLR*, 2018.
- Tuomas P. Oikarinen, Subhro Das, Lam M. Nguyen, and Tsui-Wei Weng. Label-free concept bottleneck models. In *The Eleventh International Conference on Learning Representations, ICLR*. OpenReview.net, 2023.
- Judea Pearl. Causal diagrams for empirical research. *Biometrika*, 82(4):669–688, 1995.
- Judea Pearl. Causal inference in statistics: An overview. 2009.
- Judea Pearl. Causal inference. *Causality: objectives and assessment*, pages 39–58, 2010.
- Jonas Peters, Dominik Janzing, and Bernhard Schölkopf. *Elements of causal inference: foundations and learning algorithms*. The MIT press, 2017.
- Hoifung Poon and Pedro M. Domingos. Sum-product networks: A new deep architecture. In *UAI 2011, Proceedings of the Twenty-Seventh Conference on Uncertainty in Artificial Intelligence, Barcelona, Spain, July 14-17, 2011*, pages 337–346. AUAI Press, 2011.
- Cynthia Rudin. Stop explaining black box machine learning models for high stakes decisions and use interpretable models instead. *Nat. Mach. Intell.*, 1(5):206–215, 2019.
- Karen Sachs, Omar Perez, Dana Pe’er, Douglas A Luffenburger, and Garry P Nolan. Causal protein-signaling networks derived from multiparameter single-cell data. *Science*, 308(5721):523–529, 2005.
- Marco Scutari. Learning bayesian networks with the bnlearn r package. *Journal of statistical software*, 35:1–22, 2010.
- Ivaxi Sheth, Aamer Abdul Rahman, Laya Rafiee Sevyeri, Mohammad Havaei, and Samira Ebrahimi Kahou. Learning from uncertain concepts via test time interventions. In *Workshop on trustworthy and socially responsible machine learning, NeurIPS*, 2022.
- Sungbin Shin, Yohan Jo, Sungsoo Ahn, and Namhoon Lee. A closer look at the intervention procedure of concept bottleneck models. In *International Conference on Machine Learning (ICML)*, volume 202 of *Proceedings of Machine Learning Research*, pages 31504–31520. PMLR, 2023.
- Peter Spirtes and Clark Glymour. An algorithm for fast recovery of sparse causal graphs. *Social science computer review*, 9(1):62–72, 1991.
- Divyansh Srivastava, Ge Yan, and Lily Weng. VLG-CBM: training concept bottleneck models with vision-language guidance. In *Advances in Neural Information Processing Systems 38: Annual Conference on Neural Information Processing Systems, NeurIPS*, 2024.
- Wolfgang Stammer, Patrick Schramowski, and Kristian Kersting. Right for the right concept: Revising neuro-symbolic concepts by interacting with their explanations. In *IEEE Conference on Computer Vision and Pattern Recognition, CVPR*, pages 3619–3629. Computer Vision Foundation / IEEE, 2021.

David Steinmann, Wolfgang Stammer, Felix Friedrich, and Kristian Kersting. Learning to intervene on concept bottlenecks. In *Forty-first International Conference on Machine Learning (ICML)*, volume 235 of *Proceedings of Machine Learning Research*, pages 46556–46571. PMLR / OpenReview.net, 2024.

Jin Tian and Judea Pearl. A general identification condition for causal effects. In *Proceedings of the Eighteenth National Conference on Artificial Intelligence and Fourteenth Conference on Innovative Applications of Artificial Intelligence (AAAI)*, pages 567–573. AAAI Press / The MIT Press, 2002.

Moritz Vandenhirtz, Sonia Laguna, Ricards Marcinkevics, and Julia E. Vogt. Stochastic concept bottleneck models. In *Advances in Neural Information Processing Systems 38: Annual Conference on Neural Information Processing Systems (NeurIPS)*, 2024.

Antonio Vergari, YooJung Choi, Robert Peharz, and Guy Van den Broeck. Probabilistic circuits: Representations, inference, learning and applications. *AAAI Tutorial*, 2020.

Alex Wang, Amanpreet Singh, Julian Michael, Felix Hill, Omer Levy, and Samuel R. Bowman. GLUE: A multi-task benchmark and analysis platform for natural language understanding. In *7th International Conference on Learning Representations, ICLR*. OpenReview.net, 2019.

Mert Yüksesgönül, Maggie Wang, and James Zou. Post-hoc concept bottleneck models. In *The Eleventh International Conference on Learning Representations, ICLR*. OpenReview.net, 2023.

Mateo Espinosa Zarlenga, Pietro Barbiero, Gabriele Ciravegna, Giuseppe Marra, Francesco Giannini, Michelangelo Diligenti, Zohreh Shams, Frédéric Precioso, Stefano Melacci, Adrian Weller, Pietro Lió, and Mateja Jamnik. Concept embedding models: Beyond the accuracy-explainability trade-off. In *Advances in Neural Information Processing Systems 35: Annual Conference on Neural Information Processing Systems (NeurIPS)*, 2022.

Nevin Lianwen Zhang and David L. Poole. Exploiting causal independence in bayesian network inference. *J. Artif. Intell. Res.*, 5:301–328, 1996.

Han Zhao, Pascal Poupart, and Geoffrey J. Gordon. A unified approach for learning the parameters of sum-product networks. In *NeurIPS*, pages 433–441, 2016.

---

# Causal Neural Probabilistic Circuits (Supplementary Material)

---

Weixin Chen<sup>1</sup>

Han Zhao<sup>1</sup>

<sup>1</sup>University of Illinois Urbana-Champaign, IL, USA

## A DISCUSSION

In this section, we discuss the limitations of the proposed method and outline potential solutions, which are categorized into the following three perspectives.

**Reducing Prerequisites.** In this work, we assume access to data annotated with both attribute and class labels, alongside the underlying causal graph structure over these variables. In practice, obtaining such comprehensive prerequisites can be challenging. Recent progress in LLMs and VLMs offers promising avenues for automated data annotation, as demonstrated in Oikarinen et al. [2023], Yükeşgönül et al. [2023], Srivastava et al. [2024]. Moreover, many well-established causal discovery algorithms can be used to infer potential causal graph structures, *e.g.*, Spirtes and Glymour [1991], Heckerman et al. [1995], Chickering [2002]. Since our primary goal in this work is to study how to effectively incorporate and leverage causal relationships, we operate under the assumption of full access. Nonetheless, the proposed method can be readily extended to scenarios free of attribute annotations or predefined causal graph structures.

**Improving CNPC.** We discuss the possibilities of improving CNPC from the following two perspectives.

- **Enabling the adaptive selection of  $\alpha$ :** In our main experiments, the value of  $\alpha$  is set heuristically based on whether an input instance is OOD, which reflects the reliability of the neural predictor for that instance. However, it is infeasible to manually assess the OOD status of individual instances in practice. To determine an appropriate  $\alpha$  automatically, we could leverage existing OOD detection algorithms [Hendrycks and Gimpel, 2017, Liang et al., 2018]. For example, we can design  $\alpha$  to be proportional to an OOD score that quantitatively measures the extent to which a given input deviates from the in-distribution training data. Under this mechanism, if an instance is highly likely to be OOD, CNPC will adaptively set a higher  $\alpha$  in its PoE formulation, reducing the weight of the potentially unreliable neural predictor and relying more heavily on the evidence provided by the causal PC.
- **Determining the optimal attribute intervention order:** In our main experiments, attributes are intervened upon based on their node depth in the causal graph, under the assumption that a higher-level attribute influences more downstream attributes, ultimately yielding greater improvements in predicting the target variable. However, identifying the optimal intervention set under a restricted budget (*i.e.*, a limit on the number of intervened attributes) likely depends not only on the graph topology but also on the specific causal mechanisms. For example, intervening directly on a causal parent of the target variable that exhibits a nearly deterministic causal mechanism can induce a substantial performance boost. We leave the formal derivation of the optimal attribute intervention order to future work.

**Solving More Challenging Problems.** This work primarily addresses how intervening on a specific attribute (by setting it to the ground-truth label) influences the class distribution for a given instance, *i.e.*, computing  $\Pr^{\text{do}(A_j:=a_j^*)}(Y | X = x)$ . However, researchers may also be interested in answering counterfactual questions, such as “*What would the outcome have been had the attribute been set to a different value?*”. This requires computing  $\Pr^{\text{do}(A_j:=a_j^*)}(Y | X = x, A_j = a_j^*)$ , where  $a_j^* \neq a_j$ . As noted in Section 3.3, the causal PC supports exact, tractable counterfactual inference. Therefore, future work could leverage the outputs of the causal PC to develop approximations of ground-truth counterfactual class distributions.

## B PRELIMINARIES

### B.1 CAUSAL PROBABILISTIC CIRCUITS

In this section, we elaborate on how VE schedules the factor operations (multiplication and sum-out) within a network polynomial, which in turn determines the structure of the compiled arithmetic circuit.

We continue the example from Section 3.3. That is, we consider three variables with the graph structure  $V_2 \leftarrow V_1 \rightarrow V_3$ , and apply VE with the variable elimination order  $[V_2, V_3, V_1]$ . Table 1 summarizes the VE schedule. At each step, VE collects all current factors that involve the variable to be eliminated, multiplies them, and then sums out that variable. This produces a new factor over the remaining variables, which is carried forward to subsequent steps. Specifically, the new factors produced at different steps are:  $\tau_1(V_1) = \sum_{V_2} \phi_{V_2}(V_1, V_2) \lambda_{V_2}(V_2)$ ,  $\tau_2(V_1) = \sum_{V_3} \phi_{V_3}(V_1, V_3) \lambda_{V_3}(V_3)$ , and the network polynomial  $f = \sum_{V_1} \phi_{V_1}(V_1) \tau_1(V_1) \tau_2(V_1) \lambda_{V_1}(V_1)$ .

Finding the optimal variable elimination order is known to be NP-hard. In our experiments, the variable elimination order is determined using the MinFill heuristic, which greedily selects the variable that adds the fewest new edges to the graph when eliminated.

Subsequently, the compiled arithmetic circuit is obtained by mapping each sum-out operation to a sum node and each multiplication operation to a product node, while leaf nodes correspond to symbolic parameters (the  $\phi$  entries) and indicators (the  $\lambda$  entries).

Table 1: A run of VE for the network polynomial with the elimination order  $[V_2, V_3, V_1]$ .

Step	Variable eliminated	Factors used	Variables involved	New factor
1	$V_2$	$\phi_{V_2}(V_1, V_2), \lambda_{V_2}(V_2)$	$V_1, V_2$	$\tau_1(V_1)$
2	$V_3$	$\phi_{V_3}(V_1, V_3), \lambda_{V_3}(V_3)$	$V_1, V_3$	$\tau_2(V_1)$
3	$V_1$	$\phi_{V_1}(V_1), \tau_1(V_1), \tau_2(V_1), \lambda_{V_1}(V_1)$	$V_1$	$f$

## C EXPERIMENTS

### C.1 EXPERIMENTAL SETTINGS

#### C.1.1 Datasets

Here, we provide further details regarding the data processing procedure for each dataset.

**Asia.** Following de Felice et al. [2025], we train an autoencoder to map the attribute labels into an embedding, which serves as the input to CBMs. Specifically, this autoencoder comprises two encoder layers and two decoder layers, with a latent dimension of 32. It takes a vector of all attribute labels for a given instance as input and is trained using Mean Squared Error (MSE) loss to reconstruct this vector. After training, the final instance embedding is constructed by combining 50% of the encoder’s output with 50% noise sampled from a standard normal distribution. This noise is injected to ensure the resulting embeddings are non-trivial representations of attributes. Finally, the embeddings are standardized.

**Sachs.** The Sachs dataset is processed using the identical procedure described for Asia.

**MNISTAdd.** The data-generating process for an instance in the MNISTAdd dataset proceeds in three steps. First, the value for attribute  $A_1$  (the first digit) is drawn from a uniform distribution over 0–9. Second, the value for attribute  $A_2$  (the second digit) is drawn from a highly skewed conditional distribution: with 80% probability, it is assigned the value  $(A_1 + 1)\%10$ , while the remaining 20% probability is distributed equally among the other possible digits. Finally, the class label is defined as their sum, and the instance image is formed by concatenating randomly sampled MNIST images corresponding to the sampled digit values. The causal graph depicting the relationships between the attributes and the class is illustrated in Figure 7a.

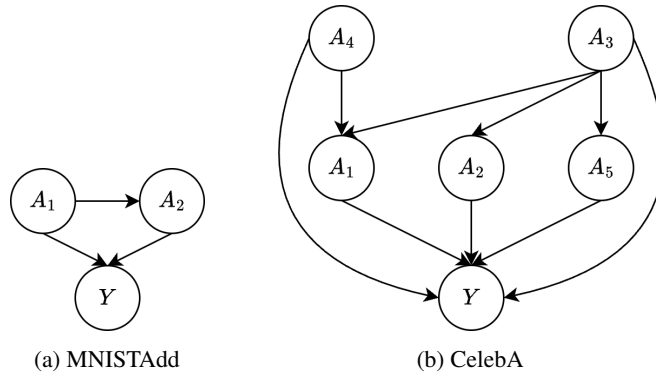


Figure 7: Causal graphs over attributes  $A_{1:K}$  and the class label  $Y$ . **Left:** The causal graph for MNISTAdd, with attributes  $A_1$ : the first digit and  $A_2$ : the second digit. **Right:** The causal graph for CelebA, with attributes  $A_1$ : Attractive,  $A_2$ : Mouth\_Slightly\_Open,  $A_3$ : Smiling,  $A_4$ : Wearing\_Lipstick, and  $A_5$ : High\_Cheekbones.

Additionally, we generate two distinct test set variants to study model performance under OOD settings: (i) We apply a 180-degree rotation to each instance. (ii) We employ the PGD attack ( $\epsilon = 8/255$ ,  $\alpha = 2/255$ , 50 steps) to generate an adversarial perturbation for each instance.

**cMNISTAdd.** The data-generating process for the cMNISTAdd dataset is similar to that for MNISTAdd, except that it introduces spurious correlations using colored digits. In the training and validation sets, the digits 0–9 are spuriously correlated with a specific list of colors; in the test set, this color-to-digit mapping is reversed. Examples of instances from the training and test sets are illustrated in Figure 8.

**CelebA.** In this paper, we focus on the five most balanced attributes in CelebA: *Attractive*, *Mouth\_Slightly\_Open*, *Smiling*, *Wearing\_Lipstick*, and *High\_Cheekbones*. We define the class label as a unique combination of these binary attributes, resulting in 32 distinct classes. Furthermore, we manually annotate the underlying causal graph over these attributes and the class label, as illustrated in Figure 7b.

Additionally, we generate two distinct test set variants to study model performance under OOD settings: (i) We apply a 180-degree rotation to each instance. (ii) We employ the PGD attack ( $\epsilon = 2/255$ ,  $\alpha = 2/255$ , 50 steps) to generate an adversarial perturbation for each instance.

### C.1.2 Implementation Details

To ensure the reliability and reproducibility of our results, we conduct all experiments across three independent trials using the random seeds 42, 52, and 62.

**CNPC.** The attribute predictor of CNPC is parameterized as a multi-task MLP consisting of a single shared hidden layer with a ReLU activation, followed by independent linear classification heads for each attribute. The hidden dimension is set to 128. We train this predictor using standard supervised learning for 100 epochs with a batch size of 256. We use the SGD optimizer with a learning rate of 0.01, a momentum of 0.9, and a weight decay of  $4e-5$ . For datasets containing image inputs, the images are resized to  $224 \times 224 \times 3$ .



Figure 8: Instances from the cMNISTAdd dataset. **Top:** Examples from the training set. **Bottom:** Examples from the test set.

**NPC.** NPC employs the attribute predictor architecture and training configuration described above. The PC serving as the label predictor is learned using LearnSPN [Gens and Domingos, 2013] and CCCP [Zhao et al., 2016]. To provide a direct comparison with CNPC, we omit the final joint training stage for the overall NPC proposed in Chen et al. [2025a].

**Vanilla CBM.** For vanilla CBM, we parameterize the concept predictor as a one-hidden-layer MLP with ReLU activation and the label predictor as a single linear layer. Specifically, we employ a vanilla CBM with an independent bottleneck (*i.e.*, the concept predictor and the label predictor are trained independently), which has been shown to achieve the highest intervention efficiency among all bottleneck types [Koh et al., 2020].

**CEM.** For CEM, we parameterize its backbone as a one-hidden-layer MLP with ReLU activation, which feeds into a concept embedding module. The resulting high-dimensional concept embeddings are concatenated and passed through a single linear layer to produce the final class prediction. The training loss for CEM is computed as the sum of the concept prediction loss and the downstream classification loss. Additionally, we adopt RandInt, a regularization strategy proposed by Zarlenga et al. [2022], which randomly performs independent concept interventions during training with a probability of  $p_{\text{int}} = 0.25$ . This strategy is designed to incentivize higher intervention efficiency during inference.

**Others.** For the model architectures and training protocols of  $C^2$ BM and SCBM, we adhere to the implementation details established by de Felice et al. [2025].

## C.2 MAIN RESULTS

### C.2.1 Benign Performance

Figure 9 illustrates the attribute accuracy (averaged across all attributes) of CNPC and baseline models in the benign setting on the Asia, Sachs, MNISTAdd, and CelebA datasets under varying numbers of attribute interventions.

Across most datasets,  $C^2$ BM leads in attribute accuracy. We attribute this to the fact that  $C^2$ BM incorporates the underlying causal graph into its neural predictor, allowing interventions to propagate through the graph structure and update downstream attribute predictions. In contrast, we focus on improving task accuracy under interventions in this work. Our proposed model, CNPC, leverages the causal relationships among attributes and the class label specifically for the final class prediction, rather than the intermediate attribute predictions. As predictions for non-intervened attributes are not updated, CNPC might not exhibit the highest attribute accuracy among all models.

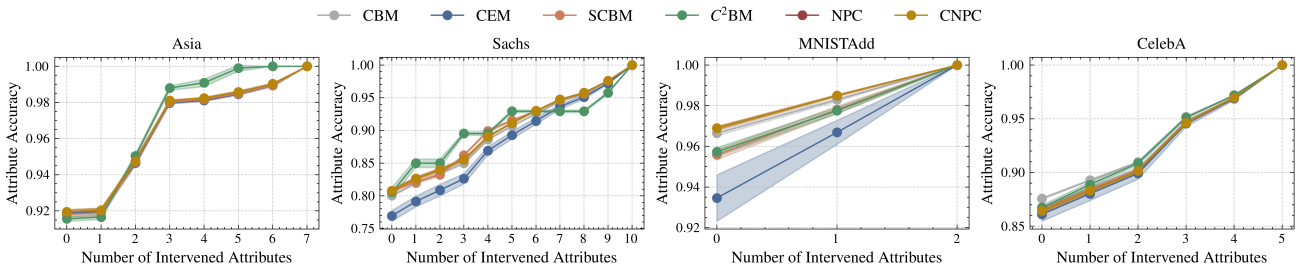


Figure 9: Attribute accuracy of CNPC and baseline models in the benign setting on the Asia, Sachs, MNISTAdd, and CelebA datasets under varying numbers of attribute interventions. All results are averaged across three random seeds.

### C.2.2 OOD Performance

Figure 10 illustrates the attribute accuracy (averaged across all attributes) of CNPC and baseline models in OOD settings on the MNISTAdd and CelebA datasets under varying numbers of attribute interventions.

Compared to the benign setting (see Figure 9), the attribute accuracy degrades substantially under OOD shifts. For instance, prior to any interventions, the unseen data transformation causes attribute accuracy to drop from over 92% to below 20% on MNISTAdd, and from over 85% to approximately 50% on CelebA. Similarly, adversarial perturbations cause attribute accuracy to drop from over 92% to below 80% on MNISTAdd, and from over 85% to below 70% on CelebA. Given

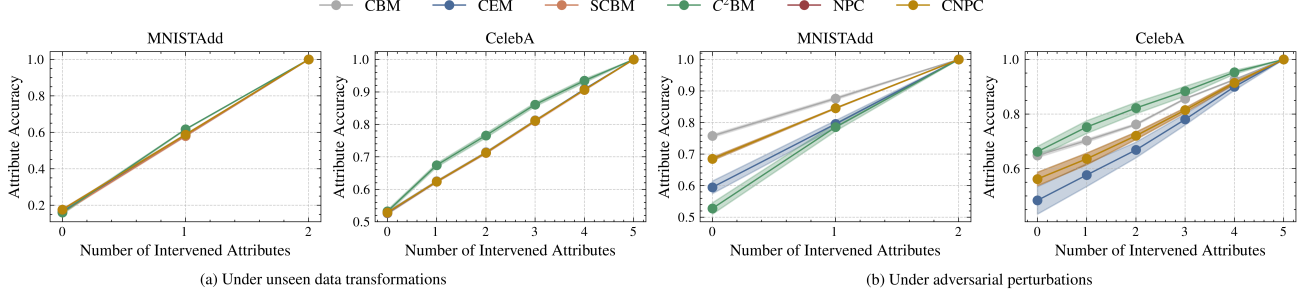


Figure 10: Attribute accuracy of CNPC and baseline models in OOD settings on the MNISTAdd and CelebA datasets under varying numbers of attribute interventions. All results are averaged across three random seeds.

this severe degradation in the neural predictor’s reliability, interventions become essential to recover downstream task performance.

## D THEORETICAL ANALYSIS

In this section, we elaborate on the proofs omitted in Section 5.

**Theorem 6** (Restatement of Theorem 3). *The expected prediction error of NPC (CNPC), measured by KL divergence, is upper-bounded by the sum of the expected prediction error of the attribute predictor and that of the PC (causal PC). Specifically,*

$$\begin{aligned} \mathbb{E}_{X \sim \mathbb{P}_*} [\text{KL}(\mathbb{P}_*(Y | X) \| \mathbb{P}_{\theta, w}(Y | X))] &\leq \mathbb{E}_{X \sim \mathbb{P}_*} [\text{KL}(\mathbb{P}_*(A_{1:K} | X) \| \mathbb{P}_{\theta}(A_{1:K} | X))] \\ &\quad + \mathbb{E}_{A_{1:K} \sim \mathbb{P}_*} [\text{KL}(\mathbb{P}_*(Y | A_{1:K}) \| \mathbb{P}_w(Y | A_{1:K}))]. \end{aligned}$$

Equality holds if for each  $(x, y)$ , there exists a constant  $c(x, y)$  such that  $\frac{\mathbb{P}_*(a_{1:K}|x)\mathbb{P}_*(y|a_{1:K})}{\mathbb{P}_{\theta}(a_{1:K}|x)\mathbb{P}_w(y|a_{1:K})} = c(x, y)$  for all  $a_{1:K}$ .

*Proof.* We proceed in three steps.

**Step 1.** Show that

$$\mathbb{E}_{X \sim \mathbb{P}_*} [\text{KL}(\mathbb{P}_*(Y | X) \| \mathbb{P}_{\theta, w}(Y | X))] = \text{KL}(\mathbb{P}_*(X, Y) \| \mathbb{P}_{\theta, w}(X, Y)),$$

where  $\mathbb{P}_{\theta, w}(X, Y) = \mathbb{P}_*(X) \mathbb{P}_{\theta, w}(Y | X)$ .

Rewriting  $\mathbb{P}_*(X, Y)$  as  $\mathbb{P}_*(X) \mathbb{P}_*(Y | X)$ , we can expand the RHS as follows.

$$\begin{aligned} \text{KL}(\mathbb{P}_*(X, Y) \| \mathbb{P}_{\theta, w}(X, Y)) &= \sum_{x, y} \mathbb{P}_*(x, y) \log \frac{\mathbb{P}_*(y | x)}{\mathbb{P}_{\theta, w}(y | x)} \\ &= \sum_x \mathbb{P}_*(x) \sum_y \mathbb{P}_*(y | x) \log \frac{\mathbb{P}_*(y | x)}{\mathbb{P}_{\theta, w}(y | x)} \\ &= \sum_x \mathbb{P}_*(x) \text{KL}(\mathbb{P}_*(Y | x) \| \mathbb{P}_{\theta, w}(Y | x)) \\ &= \mathbb{E}_{X \sim \mathbb{P}_*} [\text{KL}(\mathbb{P}_*(Y | X) \| \mathbb{P}_{\theta, w}(Y | X))]. \end{aligned}$$

**Step 2.** Show that

$$\text{KL}(\mathbb{P}_*(X, Y) \| \mathbb{P}_{\theta, w}(X, Y)) \leq \text{KL}(\mathbb{P}_*(X, A_{1:K}, Y) \| \mathbb{P}_{\theta, w}(X, A_{1:K}, Y)),$$

where  $\mathbb{P}_{\theta, w}(X, A_{1:K}, Y) = \mathbb{P}_*(X) \mathbb{P}_{\theta}(A_{1:K} | X) \mathbb{P}_w(Y | A_{1:K})$ .

Under Assumption 1,  $\mathbb{P}_{\theta, w}(x, a_{1:K}, y)$  can be written as  $\mathbb{P}_*(x) \mathbb{P}_{\theta, w}(a_{1:K}, y | x)$ ; thus, the marginal  $\sum_{a_{1:K}} \mathbb{P}_{\theta, w}(x, a_{1:K}, y)$  equals  $\mathbb{P}_{\theta, w}(x, y)$ .

Following this, we can expand the LHS as follows.

$$\begin{aligned}
\text{KL}(\mathbb{P}_*(X, Y) \parallel \mathbb{P}_{\theta, w}(X, Y)) &= \sum_{x, y} \mathbb{P}_*(x, y) \log \frac{\mathbb{P}_*(x, y)}{\mathbb{P}_{\theta, w}(x, y)} \\
&= \sum_{x, y} \left( \sum_{a_{1:K}} \mathbb{P}_*(x, a_{1:K}, y) \right) \log \frac{\sum_{a_{1:K}} \mathbb{P}_*(x, a_{1:K}, y)}{\sum_{a_{1:K}} \mathbb{P}_{\theta, w}(x, a_{1:K}, y)} \\
\text{using the log-sum inequality} &\leq \sum_{x, y} \sum_{a_{1:K}} \mathbb{P}_*(x, a_{1:K}, y) \log \frac{\mathbb{P}_*(x, a_{1:K}, y)}{\mathbb{P}_{\theta, w}(x, a_{1:K}, y)} \\
&= \text{KL}(\mathbb{P}_*(X, A_{1:K}, Y) \parallel \mathbb{P}_{\theta, w}(X, A_{1:K}, Y)).
\end{aligned}$$

Equality holds iff for each  $(x, y)$ ,  $\frac{\mathbb{P}_*(x, a_{1:K}, y)}{\mathbb{P}_{\theta, w}(x, a_{1:K}, y)}$  is some constant  $c(x, y)$  for all  $a_{1:K}$  with  $\mathbb{P}_*(x, a_{1:K}, y), \mathbb{P}_{\theta, w}(x, a_{1:K}, y) > 0$ .

**Step 3.** Decompose  $\text{KL}(\mathbb{P}_*(X, A_{1:K}, Y) \parallel \mathbb{P}_{\theta, w}(X, A_{1:K}, Y))$ .

Under Assumption 1,  $\mathbb{P}_*(X, A_{1:K}, Y)$  can be written as  $\mathbb{P}_*(X) \mathbb{P}_*(A_{1:K} \mid X) \mathbb{P}_*(Y \mid A_{1:K})$ .

Following this, we can decompose the target term as follows.

$$\begin{aligned}
\text{KL}(\mathbb{P}_*(X, A_{1:K}, Y) \parallel \mathbb{P}_{\theta, w}(X, A_{1:K}, Y)) &= \sum_{x, a_{1:K}, y} \mathbb{P}_*(x, a_{1:K}, y) \log \frac{\mathbb{P}_*(x, a_{1:K}, y)}{\mathbb{P}_{\theta, w}(x, a_{1:K}, y)} \\
&= \sum_{x, a_{1:K}, y} \mathbb{P}_*(x, a_{1:K}, y) \log \frac{\mathbb{P}_*(a_{1:K} \mid x)}{\mathbb{P}_{\theta}(a_{1:K} \mid x)} + \sum_{x, a_{1:K}, y} \mathbb{P}_*(x, a_{1:K}, y) \log \frac{\mathbb{P}_*(y \mid a_{1:K})}{\mathbb{P}_w(y \mid a_{1:K})}.
\end{aligned}$$

We use  $(*_1)$  and  $(*_2)$  to denote these two terms.

We rewrite the first term.

$$\begin{aligned}
(*_1) &= \sum_{x, a_{1:K}} \mathbb{P}_*(x, a_{1:K}) \log \frac{\mathbb{P}_*(a_{1:K} \mid x)}{\mathbb{P}_{\theta}(a_{1:K} \mid x)} \\
&= \sum_x \mathbb{P}_*(x) \sum_{a_{1:K}} \mathbb{P}_*(a_{1:K} \mid x) \log \frac{\mathbb{P}_*(a_{1:K} \mid x)}{\mathbb{P}_{\theta}(a_{1:K} \mid x)} \\
&= \sum_x \mathbb{P}_*(x) \text{KL}(\mathbb{P}_*(A_{1:K} \mid x) \parallel \mathbb{P}_{\theta}(A_{1:K} \mid x)) \\
&= \mathbb{E}_{X \sim \mathbb{P}_*} [\text{KL}(\mathbb{P}_*(A_{1:K} \mid X) \parallel \mathbb{P}_{\theta}(A_{1:K} \mid X))].
\end{aligned}$$

We also rewrite the second term.

$$\begin{aligned}
(*_2) &= \sum_{x, a_{1:K}} \mathbb{P}_*(x, a_{1:K}) \sum_y \mathbb{P}_*(y \mid a_{1:K}) \log \frac{\mathbb{P}_*(y \mid a_{1:K})}{\mathbb{P}_w(y \mid a_{1:K})} \\
&= \sum_{x, a_{1:K}} \mathbb{P}_*(x, a_{1:K}) \text{KL}(\mathbb{P}_*(Y \mid a_{1:K}) \parallel \mathbb{P}_w(Y \mid a_{1:K})) \\
&= \sum_{a_{1:K}} \mathbb{P}_*(a_{1:K}) \text{KL}(\mathbb{P}_*(Y \mid a_{1:K}) \parallel \mathbb{P}_w(Y \mid a_{1:K})) \\
&= \mathbb{E}_{A_{1:K} \sim \mathbb{P}_*} [\text{KL}(\mathbb{P}_*(Y \mid A_{1:K}) \parallel \mathbb{P}_w(Y \mid A_{1:K}))].
\end{aligned}$$

Summarizing the three steps, we have:

$$\begin{aligned}
\mathbb{E}_{X \sim \mathbb{P}_*} [\text{KL}(\mathbb{P}_*(Y \mid X) \parallel \mathbb{P}_{\theta, w}(Y \mid X))] &\leq \mathbb{E}_{X \sim \mathbb{P}_*} [\text{KL}(\mathbb{P}_*(A_{1:K} \mid X) \parallel \mathbb{P}_{\theta}(A_{1:K} \mid X))] \\
&\quad + \mathbb{E}_{A_{1:K} \sim \mathbb{P}_*} [\text{KL}(\mathbb{P}_*(Y \mid A_{1:K}) \parallel \mathbb{P}_w(Y \mid A_{1:K}))].
\end{aligned}$$

Equality holds iff for each  $(x, y)$ ,  $\frac{\mathbb{P}_*(x, a_{1:K}, y)}{\mathbb{P}_{\theta, w}(x, a_{1:K}, y)} = \frac{\mathbb{P}_*(a_{1:K} \mid x) \mathbb{P}_*(y \mid a_{1:K})}{\mathbb{P}_{\theta}(a_{1:K} \mid x) \mathbb{P}_w(y \mid a_{1:K})}$  is some constant  $c(x, y)$  for all  $a_{1:K}$  with  $\mathbb{P}_*(x, a_{1:K}, y), \mathbb{P}_{\theta, w}(x, a_{1:K}, y) > 0$ .

□

**Corollary 7** (Restatement of Corollary 4). *The expected interventional error of NPC is upper-bounded by the sum of the expected interventional error of the attribute predictor and the expected prediction error of the PC. Specifically,*

$$\begin{aligned} \mathbb{E}_{X \sim \mathbb{P}_*^{\text{do}_j}} \left[ \text{KL} \left( \mathbb{P}_*^{\text{do}_j}(Y | X) \parallel \mathbb{P}_{\theta, w}^{\text{do}_j}(Y | X) \right) \right] &\leq \mathbb{E}_{X \sim \mathbb{P}_*^{\text{do}_j}} \left[ \text{KL} \left( \mathbb{P}_*^{\text{do}_j}(A_{1:K} | X) \parallel \mathbb{P}_{\theta}^{\text{do}_j}(A_{1:K} | X) \right) \right] \\ &+ \mathbb{E}_{A_{1:K} \sim \mathbb{P}_*^{\text{do}_j}} \left[ \text{KL} \left( \mathbb{P}_*(Y | A_{1:K}) \parallel \mathbb{P}_w(Y | A_{1:K}) \right) \right]. \end{aligned}$$

Equality holds if for each  $(x, y)$ , there exists a constant  $c(x, y)$  such that  $\frac{\mathbb{P}_*^{\text{do}_j}(a_{1:K}|x)\mathbb{P}_*(y|a_{1:K})}{\mathbb{P}_{\theta}^{\text{do}_j}(a_{1:K}|x)\mathbb{P}_w(y|a_{1:K})} = c(x, y)$  for all  $a_{1:K}$ .

*Proof.* This result is a corollary of Theorem 3. The proof follows the same steps, except that all distributions are taken under the intervention. For completeness, we still spell out the three steps below.

**Step 1.** Show that

$$\mathbb{E}_{X \sim \mathbb{P}_*^{\text{do}_j}} \left[ \text{KL} \left( \mathbb{P}_*^{\text{do}_j}(Y | X) \parallel \mathbb{P}_{\theta, w}^{\text{do}_j}(Y | X) \right) \right] = \text{KL} \left( \mathbb{P}_*^{\text{do}_j}(X, Y) \parallel \mathbb{P}_{\theta, w}^{\text{do}_j}(X, Y) \right),$$

where  $\mathbb{P}_{\theta, w}^{\text{do}_j}(X, Y) = \mathbb{P}_*^{\text{do}_j}(X) \mathbb{P}_{\theta, w}^{\text{do}_j}(Y | X)$ .

Rewriting  $\mathbb{P}_*^{\text{do}_j}(X, Y)$  as  $\mathbb{P}_*^{\text{do}_j}(X) \mathbb{P}_*^{\text{do}_j}(Y | X)$ , we can expand the RHS as follows.

$$\begin{aligned} \text{KL} \left( \mathbb{P}_*^{\text{do}_j}(X, Y) \parallel \mathbb{P}_{\theta, w}^{\text{do}_j}(X, Y) \right) &= \sum_{x, y} \mathbb{P}_*^{\text{do}_j}(x, y) \log \frac{\mathbb{P}_*^{\text{do}_j}(y | x)}{\mathbb{P}_{\theta, w}^{\text{do}_j}(y | x)} \\ &= \sum_x \mathbb{P}_*^{\text{do}_j}(x) \sum_y \mathbb{P}_*^{\text{do}_j}(y | x) \log \frac{\mathbb{P}_*^{\text{do}_j}(y | x)}{\mathbb{P}_{\theta, w}^{\text{do}_j}(y | x)} \\ &= \sum_x \mathbb{P}_*^{\text{do}_j}(x) \text{KL} \left( \mathbb{P}_*^{\text{do}_j}(Y | x) \parallel \mathbb{P}_{\theta, w}^{\text{do}_j}(Y | x) \right) \\ &= \mathbb{E}_{X \sim \mathbb{P}_*^{\text{do}_j}} \left[ \text{KL} \left( \mathbb{P}_*^{\text{do}_j}(Y | X) \parallel \mathbb{P}_{\theta, w}^{\text{do}_j}(Y | X) \right) \right]. \end{aligned}$$

**Step 2.** Show that

$$\text{KL} \left( \mathbb{P}_*^{\text{do}_j}(X, Y) \parallel \mathbb{P}_{\theta, w}^{\text{do}_j}(X, Y) \right) \leq \text{KL} \left( \mathbb{P}_*^{\text{do}_j}(X, A_{1:K}, Y) \parallel \mathbb{P}_{\theta, w}^{\text{do}_j}(X, A_{1:K}, Y) \right),$$

where  $\mathbb{P}_{\theta, w}^{\text{do}_j}(X, A_{1:K}, Y) = \mathbb{P}_*^{\text{do}_j}(X) \mathbb{P}_{\theta}^{\text{do}_j}(A_{1:K} | X) \mathbb{P}_w^{\text{do}_j}(Y | A_{1:K})$ .

Under Assumption 1,  $\mathbb{P}_{\theta, w}^{\text{do}_j}(x, a_{1:K}, y)$  can be written as  $\mathbb{P}_*^{\text{do}_j}(x) \mathbb{P}_{\theta, w}^{\text{do}_j}(a_{1:K}, y | x)$ ; thus, the marginal  $\sum_{a_{1:K}} \mathbb{P}_{\theta, w}^{\text{do}_j}(x, a_{1:K}, y)$  equals  $\mathbb{P}_{\theta, w}^{\text{do}_j}(x, y)$ .

Following this, we can expand the LHS as follows.

$$\begin{aligned} \text{KL} \left( \mathbb{P}_*^{\text{do}_j}(X, Y) \parallel \mathbb{P}_{\theta, w}^{\text{do}_j}(X, Y) \right) &= \sum_{x, y} \mathbb{P}_*^{\text{do}_j}(x, y) \log \frac{\mathbb{P}_*^{\text{do}_j}(x, y)}{\mathbb{P}_{\theta, w}^{\text{do}_j}(x, y)} \\ &= \sum_{x, y} \left( \sum_{a_{1:K}} \mathbb{P}_*^{\text{do}_j}(x, a_{1:K}, y) \right) \log \frac{\sum_{a_{1:K}} \mathbb{P}_*^{\text{do}_j}(x, a_{1:K}, y)}{\sum_{a_{1:K}} \mathbb{P}_{\theta, w}^{\text{do}_j}(x, a_{1:K}, y)} \\ \text{using the log-sum inequality} &\leq \sum_{x, y} \sum_{a_{1:K}} \mathbb{P}_*^{\text{do}_j}(x, a_{1:K}, y) \log \frac{\mathbb{P}_*^{\text{do}_j}(x, a_{1:K}, y)}{\mathbb{P}_{\theta, w}^{\text{do}_j}(x, a_{1:K}, y)} \\ &= \text{KL} \left( \mathbb{P}_*^{\text{do}_j}(X, A_{1:K}, Y) \parallel \mathbb{P}_{\theta, w}^{\text{do}_j}(X, A_{1:K}, Y) \right). \end{aligned}$$

Equality holds iff for each  $(x, y)$ ,  $\frac{\mathbb{P}_*^{\text{do}_j}(x, a_{1:K}, y)}{\mathbb{P}_{\theta, w}^{\text{do}_j}(x, a_{1:K}, y)}$  is some constant  $c(x, y)$  for all  $a_{1:K}$  with  $\mathbb{P}_*^{\text{do}_j}(x, a_{1:K}, y), \mathbb{P}_{\theta, w}^{\text{do}_j}(x, a_{1:K}, y) > 0$ .

**Step 3.** Decompose  $\text{KL}\left(\mathbb{P}_*^{\text{do}_j}(X, A_{1:K}, Y) \parallel \mathbb{P}_{\theta, w}^{\text{do}_j}(X, A_{1:K}, Y)\right)$ .

Under Assumption 1,  $\mathbb{P}_*^{\text{do}_j}(X, A_{1:K}, Y)$  can be written as  $\mathbb{P}_*^{\text{do}_j}(X) \mathbb{P}_*^{\text{do}_j}(A_{1:K} \mid X) \mathbb{P}_*^{\text{do}_j}(Y \mid A_{1:K})$ .

Following this, we can decompose the target term as follows.

$$\begin{aligned} \text{KL}\left(\mathbb{P}_*^{\text{do}_j}(X, A_{1:K}, Y) \parallel \mathbb{P}_{\theta, w}^{\text{do}_j}(X, A_{1:K}, Y)\right) &= \sum_{x, a_{1:K}, y} \mathbb{P}_*^{\text{do}_j}(x, a_{1:K}, y) \log \frac{\mathbb{P}_*^{\text{do}_j}(x, a_{1:K}, y)}{\mathbb{P}_{\theta, w}^{\text{do}_j}(x, a_{1:K}, y)} \\ &= \sum_{x, a_{1:K}, y} \mathbb{P}_*^{\text{do}_j}(x, a_{1:K}, y) \log \frac{\mathbb{P}_*^{\text{do}_j}(a_{1:K} \mid x)}{\mathbb{P}_{\theta}^{\text{do}_j}(a_{1:K} \mid x)} + \sum_{x, a_{1:K}, y} \mathbb{P}_*^{\text{do}_j}(x, a_{1:K}, y) \log \frac{\mathbb{P}_*^{\text{do}_j}(y \mid a_{1:K})}{\mathbb{P}_w^{\text{do}_j}(y \mid a_{1:K})} \end{aligned}$$

We use  $(*_1)$  and  $(*_2)$  to denote these two terms.

We rewrite the first term.

$$\begin{aligned} (*_1) &= \sum_{x, a_{1:K}} \mathbb{P}_*^{\text{do}_j}(x, a_{1:K}) \log \frac{\mathbb{P}_*^{\text{do}_j}(a_{1:K} \mid x)}{\mathbb{P}_{\theta}^{\text{do}_j}(a_{1:K} \mid x)} \\ &= \sum_x \mathbb{P}_*^{\text{do}_j}(x) \sum_{a_{1:K}} \mathbb{P}_*^{\text{do}_j}(a_{1:K} \mid x) \log \frac{\mathbb{P}_*^{\text{do}_j}(a_{1:K} \mid x)}{\mathbb{P}_{\theta}^{\text{do}_j}(a_{1:K} \mid x)} \\ &= \sum_x \mathbb{P}_*^{\text{do}_j}(x) \text{KL}\left(\mathbb{P}_*^{\text{do}_j}(A_{1:K} \mid x) \parallel \mathbb{P}_{\theta}^{\text{do}_j}(A_{1:K} \mid x)\right) \\ &= \mathbb{E}_{X \sim \mathbb{P}_*^{\text{do}_j}} \left[ \text{KL}\left(\mathbb{P}_*^{\text{do}_j}(A_{1:K} \mid X) \parallel \mathbb{P}_{\theta}^{\text{do}_j}(A_{1:K} \mid X)\right) \right]. \end{aligned}$$

By assumption,  $\text{Pa}_C(Y) \subseteq \{A_{1:K}\} \subseteq \text{ND}_C(Y)$ . Hence, by the local Markov property and the invariance of causal mechanisms, we have:

$$\begin{aligned} \mathbb{P}_*(Y \mid A_{1:K}) &= \mathbb{P}_*(Y \mid \text{Pa}(Y)), \\ \mathbb{P}_*^{\text{do}_j}(Y \mid A_{1:K}) &= \mathbb{P}_*^{\text{do}_j}(Y \mid \text{Pa}(Y)), \\ \mathbb{P}_*(Y \mid \text{Pa}(Y)) &= \mathbb{P}_*^{\text{do}_j}(Y \mid \text{Pa}(Y)). \end{aligned}$$

Consequently,  $\mathbb{P}_*(Y \mid A_{1:K}) = \mathbb{P}_*^{\text{do}_j}(Y \mid A_{1:K})$ , and similarly,  $\mathbb{P}_w(Y \mid A_{1:K}) = \mathbb{P}_w^{\text{do}_j}(Y \mid A_{1:K})$ . Thus, the second term can be written as:

$$\begin{aligned} (*_2) &= \sum_{x, a_{1:K}} \mathbb{P}_*^{\text{do}_j}(x, a_{1:K}) \sum_y \mathbb{P}_*^{\text{do}_j}(y \mid a_{1:K}) \log \frac{\mathbb{P}_*^{\text{do}_j}(y \mid a_{1:K})}{\mathbb{P}_w^{\text{do}_j}(y \mid a_{1:K})} \\ &= \sum_{x, a_{1:K}} \mathbb{P}_*^{\text{do}_j}(x, a_{1:K}) \sum_y \mathbb{P}_*(y \mid a_{1:K}) \log \frac{\mathbb{P}_*(y \mid a_{1:K})}{\mathbb{P}_w(y \mid a_{1:K})} \\ &= \sum_{x, a_{1:K}} \mathbb{P}_*^{\text{do}_j}(x, a_{1:K}) \text{KL}\left(\mathbb{P}_*(Y \mid a_{1:K}) \parallel \mathbb{P}_w(Y \mid a_{1:K})\right) \\ &= \sum_{a_{1:K}} \mathbb{P}_*^{\text{do}_j}(a_{1:K}) \text{KL}\left(\mathbb{P}_*(Y \mid a_{1:K}) \parallel \mathbb{P}_w(Y \mid a_{1:K})\right) \\ &= \mathbb{E}_{A_{1:K} \sim \mathbb{P}_*^{\text{do}_j}} \left[ \text{KL}\left(\mathbb{P}_*(Y \mid A_{1:K}) \parallel \mathbb{P}_w(Y \mid A_{1:K})\right) \right] \end{aligned}$$

Summarizing the three steps, we have:

$$\begin{aligned} \mathbb{E}_{X \sim \mathbb{P}_*^{\text{do}_j}} \left[ \text{KL}\left(\mathbb{P}_*^{\text{do}_j}(Y \mid X) \parallel \mathbb{P}_{\theta, w}^{\text{do}_j}(Y \mid X)\right) \right] &\leq \mathbb{E}_{X \sim \mathbb{P}_*^{\text{do}_j}} \left[ \text{KL}\left(\mathbb{P}_*^{\text{do}_j}(A_{1:K} \mid X) \parallel \mathbb{P}_{\theta}^{\text{do}_j}(A_{1:K} \mid X)\right) \right] \\ &\quad + \mathbb{E}_{A_{1:K} \sim \mathbb{P}_*^{\text{do}_j}} \left[ \text{KL}\left(\mathbb{P}_*(Y \mid A_{1:K}) \parallel \mathbb{P}_w(Y \mid A_{1:K})\right) \right]. \end{aligned}$$

Equality holds iff for each  $(x, y)$ ,  $\frac{\mathbb{P}_*^{\text{do}_j}(x, a_{1:K}, y)}{\mathbb{P}_{\theta, w}^{\text{do}_j}(x, a_{1:K}, y)} = \frac{\mathbb{P}_*^{\text{do}_j}(a_{1:K} \mid x) \mathbb{P}_*^{\text{do}_j}(y \mid a_{1:K})}{\mathbb{P}_{\theta}^{\text{do}_j}(a_{1:K} \mid x) \mathbb{P}_w^{\text{do}_j}(y \mid a_{1:K})} = \frac{\mathbb{P}_*^{\text{do}_j}(a_{1:K} \mid x) \mathbb{P}_*(y \mid a_{1:K})}{\mathbb{P}_{\theta}^{\text{do}_j}(a_{1:K} \mid x) \mathbb{P}_w(y \mid a_{1:K})}$  is some constant  $c(x, y)$

for all  $a_{1:K}$  with  $\mathbb{P}_*^{\text{do}_j}(x, a_{1:K}, y), \mathbb{P}_{\theta, w}^{\text{do}_j}(x, a_{1:K}, y) > 0$ .

□

**Corollary 8** (Restatement of Corollary 5). *The expected interventional error of CNPC is upper-bounded by a weighted sum of (i) the expected interventional error of the attribute predictor, (ii) the expected interventional error of the causal PC over attributes, and (iii) the expected prediction error of the causal PC. Specifically,*

$$\begin{aligned} \mathbb{E}_{X \sim \mathbb{P}_*^{\text{do}_j}} \left[ \text{KL} \left( \mathbb{P}_*^{\text{do}_j}(Y | X) \parallel \tilde{\mathbb{P}}_{\theta, w, \alpha}^{\text{do}_j}(Y | X) \right) \right] &\leq (1 - \alpha) \mathbb{E}_{X \sim \mathbb{P}_*^{\text{do}_j}} \left[ \text{KL} \left( \mathbb{P}_*^{\text{do}_j}(A_{1:K} | X) \parallel \mathbb{P}_\theta^{\text{do}_j}(A_{1:K} | X) \right) \right] \\ &+ \alpha \mathbb{E}_{X \sim \mathbb{P}_*^{\text{do}_j}} \left[ \text{KL} \left( \mathbb{P}_*^{\text{do}_j}(A_{1:K} | X) \parallel \mathbb{P}_w^{\text{do}_j}(A_{1:K}) \right) \right] \\ &+ \mathbb{E}_{A_{1:K} \sim \mathbb{P}_*^{\text{do}_j}} \left[ \text{KL} \left( \mathbb{P}_*(Y | A_{1:K}) \parallel \mathbb{P}_w(Y | A_{1:K}) \right) \right]. \end{aligned}$$

Equality holds if for each  $(x, y)$ ,  $\mathbb{P}_\theta^{\text{do}_j}(a_{1:K} | x) = \mathbb{P}_w^{\text{do}_j}(a_{1:K})$  for all  $a_{1:K}$ , and there exists a constant  $c(x, y)$  such that  $\frac{\mathbb{P}_*^{\text{do}_j}(a_{1:K}|x)\mathbb{P}_*(y|a_{1:K})}{\tilde{\mathbb{P}}_{\theta, w, \alpha}^{\text{do}_j}(a_{1:K}|x)\mathbb{P}_w(y|a_{1:K})} = c(x, y)$  for all  $a_{1:K}$ .

*Proof.* Following the three steps outlined in the proof of Corollary 4, we obtain:

$$\begin{aligned} \mathbb{E}_{X \sim \mathbb{P}_*^{\text{do}_j}} \left[ \text{KL} \left( \mathbb{P}_*^{\text{do}_j}(Y | X) \parallel \tilde{\mathbb{P}}_{\theta, w, \alpha}^{\text{do}_j}(Y | X) \right) \right] &\leq \mathbb{E}_{X \sim \mathbb{P}_*^{\text{do}_j}} \left[ \text{KL} \left( \mathbb{P}_*^{\text{do}_j}(A_{1:K} | X) \parallel \tilde{\mathbb{P}}_{\theta, w, \alpha}^{\text{do}_j}(A_{1:K} | X) \right) \right] \\ &+ \mathbb{E}_{A_{1:K} \sim \mathbb{P}_*^{\text{do}_j}} \left[ \text{KL} \left( \mathbb{P}_*(Y | A_{1:K}) \parallel \mathbb{P}_w(Y | A_{1:K}) \right) \right]. \end{aligned}$$

Equality holds iff for each  $(x, y)$ ,  $\frac{\mathbb{P}_*^{\text{do}_j}(x, a_{1:K}, y)}{\tilde{\mathbb{P}}_{\theta, w, \alpha}^{\text{do}_j}(x, a_{1:K}, y)}$  is some constant  $c(x, y)$  for all  $a_{1:K}$  with  $\mathbb{P}_*^{\text{do}_j}(x, a_{1:K}, y), \tilde{\mathbb{P}}_{\theta, w, \alpha}^{\text{do}_j}(x, a_{1:K}, y) > 0$ .

Here, we apply an additional step to decompose  $\mathbb{E}_{X \sim \mathbb{P}_*^{\text{do}_j}} \left[ \text{KL} \left( \mathbb{P}_*^{\text{do}_j}(A_{1:K} | X) \parallel \tilde{\mathbb{P}}_{\theta, w, \alpha}^{\text{do}_j}(A_{1:K} | X) \right) \right]$ .

$$\begin{aligned} \text{KL} \left( \mathbb{P}_*^{\text{do}_j}(A_{1:K} | X) \parallel \tilde{\mathbb{P}}_{\theta, w, \alpha}^{\text{do}_j}(A_{1:K} | X) \right) &= (1 - \alpha) \text{KL} \left( \mathbb{P}_*^{\text{do}_j}(A_{1:K} | X) \parallel \mathbb{P}_\theta^{\text{do}_j}(A_{1:K} | X) \right) \\ &+ \alpha \text{KL} \left( \mathbb{P}_*^{\text{do}_j}(A_{1:K} | X) \parallel \mathbb{P}_w^{\text{do}_j}(A_{1:K}) \right) \\ &+ \log Z_\alpha(X) \end{aligned}$$

By Hölder's inequality,  $\log Z_\alpha(X)$  can be written as:

$$\begin{aligned} \log Z_\alpha(X) &= \log \sum_{a_{1:K}} \left( \mathbb{P}_\theta^{\text{do}_j}(A_{1:K} = a_{1:K} | X) \right)^{1-\alpha} \left( \mathbb{P}_w^{\text{do}_j}(A_{1:K} = a_{1:K}) \right)^\alpha \\ &\leq \log \left( \sum_{a_{1:K}} \mathbb{P}_\theta^{\text{do}_j}(A_{1:K} = a_{1:K} | X) \right)^{1-\alpha} \left( \sum_{a_{1:K}} \mathbb{P}_w^{\text{do}_j}(A_{1:K} = a_{1:K}) \right)^\alpha \\ &= 0 \end{aligned}$$

Equality holds when  $\frac{\mathbb{P}_\theta^{\text{do}_j}(A_{1:K}=a_{1:K}|X)}{\mathbb{P}_w^{\text{do}_j}(A_{1:K}=a_{1:K})} = 1$  for all  $a_{1:K}$ .

Summarizing all steps, we have:

$$\begin{aligned} \mathbb{E}_{X \sim \mathbb{P}_*^{\text{do}_j}} \left[ \text{KL} \left( \mathbb{P}_*^{\text{do}_j}(Y | X) \parallel \tilde{\mathbb{P}}_{\theta, w, \alpha}^{\text{do}_j}(Y | X) \right) \right] &\leq (1 - \alpha) \mathbb{E}_{X \sim \mathbb{P}_*^{\text{do}_j}} \left[ \text{KL} \left( \mathbb{P}_*^{\text{do}_j}(A_{1:K} | X) \parallel \mathbb{P}_\theta^{\text{do}_j}(A_{1:K} | X) \right) \right] \\ &+ \alpha \mathbb{E}_{X \sim \mathbb{P}_*^{\text{do}_j}} \left[ \text{KL} \left( \mathbb{P}_*^{\text{do}_j}(A_{1:K} | X) \parallel \mathbb{P}_w^{\text{do}_j}(A_{1:K}) \right) \right] \\ &+ \mathbb{E}_{A_{1:K} \sim \mathbb{P}_*^{\text{do}_j}} \left[ \text{KL} \left( \mathbb{P}_*(Y | A_{1:K}) \parallel \mathbb{P}_w(Y | A_{1:K}) \right) \right]. \end{aligned}$$

Equality holds iff for each  $(x, y)$ ,  $\mathbb{P}_\theta^{\text{do}_j}(a_{1:K} | x) = \mathbb{P}_w^{\text{do}_j}(a_{1:K})$  for all  $a_{1:K}$ , and  $\frac{\mathbb{P}_*^{\text{do}_j}(x, a_{1:K}, y)}{\tilde{\mathbb{P}}_{\theta, w, \alpha}^{\text{do}_j}(x, a_{1:K}, y)} = \frac{\mathbb{P}_*^{\text{do}_j}(a_{1:K}|x)\mathbb{P}_*(y|a_{1:K})}{\tilde{\mathbb{P}}_{\theta, w, \alpha}^{\text{do}_j}(a_{1:K}|x)\mathbb{P}_w(y|a_{1:K})} = \frac{\mathbb{P}_*^{\text{do}_j}(a_{1:K}|x)\mathbb{P}_*(y|a_{1:K})}{\mathbb{P}_\theta^{\text{do}_j}(a_{1:K}|x)\mathbb{P}_w^{\text{do}_j}(y|a_{1:K})} = \frac{\mathbb{P}_*^{\text{do}_j}(a_{1:K}|x)\mathbb{P}_*(y|a_{1:K})}{\mathbb{P}_\theta^{\text{do}_j}(a_{1:K}|x)\mathbb{P}_w(y|a_{1:K})}$  is some constant  $c(x, y)$  for all  $a_{1:K}$  with  $\mathbb{P}_*^{\text{do}_j}(x, a_{1:K}, y), \tilde{\mathbb{P}}_{\theta, w, \alpha}^{\text{do}_j}(x, a_{1:K}, y) > 0$ .

□